Advances in Water Resources 000 (2017) 1–15

Contents lists available at ScienceDirect

Advances in Water Resources

journal homepage: www.elsevier.com/locate/advwatres

Equivalence of turbulence statistics between monodisperse and polydisperse turbidity currents

Mrugesh Shringarpure[a,b,*], Mariano I. Cantero[c,d,e], S. Balachandar[a]

[a] Department of Mechanical and Aerospace Engineering, University of Florida, Gainesville, FL, USA
[b] ExxonMobil Upstream Research Company, Spring, TX, USA
[c] Instituto Balseiro, Universidad Nacional de Cuyo, San Carlos de Bariloche, Río Negro, Argentina
[d] Centro Atómico Bariloche, Comisión Nacional de Energía Atómica, San Carlos de Bariloche, Río Negro, Argentina
[e] Consejo Nacional de Investigaciones Científicas y Técnicas, San Carlos de Bariloche, Río Negro, Argentina

ARTICLE INFO

Article history:
Received 30 January 2017
Revised 16 May 2017
Accepted 19 May 2017
Available online xxx

MSC:
00-01
99-00

Keywords:
Turbidity currents
Polydisperse suspensions
Turbulence
Multiphase flows

ABSTRACT

Turbidity currents are buoyancy driven submarine flows where the source of buoyancy is typically a polydisperse sediment suspension. Sustained propagation of such flows depend on the ability of turbulence in the flow to keep the settling sediments in suspension. Recent studies by Cantero et al. (2012b) and Shringarpure et al. (2012) have investigated the interaction of monodisperse sediment suspension and turbulence in turbidity currents on smooth sloping beds. These studies showed that stable stratification of sediment suspension damps turbulence and in some cases can be fully suppress turbulence. Furthermore, it was shown that the turbulence damping effect of a monodisperse sediment suspension can be quantified by the product of shear Richardson number and the sediment settling velocity. In this study we generalize this result for a polydisperse sediment suspension. We compare the turbulence statistics of turbidity currents driven by different polydisperse suspensions and show that as long as the total amount of sediment and the product of shear Richardson number and effective settling velocity (a value representing the polydisperse suspension) are the same, the turbulent velocity statistics of the different polydisperse suspensions nearly collapse. Furthermore, if the effective settling velocity is chosen to be depth-dependent (a function of height from the bed) then the turbulence statistics involving sediment concentration also collapses between different polydisperse suspensions. These results suggest the possibility of modeling polydisperse currents with an equivalent monodisperse suspension whose total sediment load and depth-dependent settling velocity match those of the polydisperse suspension.

1. Introduction

Typically, turbidity currents are characterized as highly turbulent flows driven by dilute concentration of suspended sediments (Allen, 2001; Kneller and Buckee, 2000; Parsons et al., 2009). These flows are extremely energetic (Krause et al., 1970; Prior et al., 1987), travel long distances (Kneller and Buckee, 2000) and are an important sediment transport mechanism in the submarine world (García, 1992; Parsons et al., 2009). Field scale turbidity currents are complex, spatially and temporally evolving flows. Several factors like ambient conditions (stratification, salinity), bed topography (slope, roughness and shape), bed conditions (particle size distribution, cohesive effects, compaction), and description of the sediment suspension driving the flow (particle size distribution, total suspended load) have varying influence on the flow.

A turbidity current can be divided into three regions - head, body and a tail (Allen, 2001; Simpson, 1997; Ungarish, 2009). The head is the most energetic part, characterized as highly turbulent with intense mixing (Cantero et al., 2007a; 2007b; Hartel et al., 2000; Necker et al., 2005; Patterson et al., 2006). It can be extremely erosive and rework the bed (Cantero et al., 2008b). However, from the perspective of a fixed point on the bed, the head passes over it quickly and therefore its effect lasts only for a short duration. The tail of a turbidity current is a weak and depositional flow (Kneller et al., 1997). The body of a turbidity current is a region of transition from the highly turbulent head to a weak depositional tail. It must be noted that the head and tail will always exist, however, the existence of a distinct body is determined by various factors like the bed conditions and sediment load at the time of flow inception. Nevertheless the body is considered to be the main manifestation of a turbidity current and a primary mechanism for sediment transport.

* Corresponding author at: ExxonMobil Upstream Research Company, Spring, TX, USA.
E-mail address: mrugesh.s.shringarpure@exxonmobil.com (M. Shringarpure).

http://dx.doi.org/10.1016/j.advwatres.2017.05.015
0309-1708/

In the past several decades there has been an intensive effort to study various regions and aspects of turbidity currents. These studies range from laboratory experiments (Bonnecaze et al., 1995; 1996; Garcia and Parker, 1993; Sequeiros et al., 2010) to field observations (Talling et al., 2007; Xu et al., 2004). Great effort has also been devoted to numerical simulations of turbidity currents, with emphasis on studying the flow dynamics (Cantero et al., 2007a; 2008a; 2005; 2007b; Das et al., 2004; Hartel et al., 2000; Imran et al., 2004), turbulent structures (Cantero et al., 2008b), turbulence modulation (Cantero et al., 2014; 2009b) and topographical effects of the sea bed (Cantero et al., 2012a; Nasr-Azadani et al., 2013; Nasr-Azadani and Meiburg, 2014). Theoretical analysis has given conditions for self-accelerating and auto-suspension turbidity currents (Bagnold, 1962; Fukushima et al., 1985; Pantin, 1979; Pantin and Franklin, 2009; Parker et al., 1986) and also proposed reduced or simplified (box) models for simulating and analyzing such flows (see Parker et al. (1986) for shallow water equations and Bonnecaze et al. (1995) for box models). Experiments have been performed to validate some of these theoretical predictions (Sequeiros et al., 2009). More recently Cantero et al. (2009a) and Shringarpure et al. (2012) employed Direct Numerical Simulations to study the dynamics of the flow in the body of turbidity currents in greater detail. Up-to-date, the study of the dynamics of polydisperse turbidity currents has received limited attention. Recently, Nasr-Azadani et al. (2013) and Nasr-Azadani and Meiburg (2014) investigated the effect of polydisperse lock exchange currents on bed topography by performing experiments and numerical simulations.

In turbidity currents the sediment suspension has two effects on the flow – it drives the flow (which generates turbulence) due to the imposed excess density and the settling sediment particles preferentially segregates in the flow leading to a stable stratification of sediment concentration which damps turbulence. The driving effect of suspended sediments is proportional to the total volumetric concentration of sediment. On the other hand, the damping effect on turbulence can be viewed as the total turbulent kinetic energy spent by the flow to keep the settling sediment particles in suspension. Cantero et al. (2012b) showed that the damping effect in a monodisperse turbidity current is controlled by the product of shear Richardson number (Ri_τ) and settling velocity of the sediment ($\tilde{V}\cos\theta$). Here $\tilde{V}$ is the dimensionless settling velocity of a sediment particle in still fluid and θ is the bed angle with the horizontal direction. This parametric grouping was extended to bi-disperse suspensions (Shringarpure et al. (2014, 2015) where it takes the form $Ri_\tau(\gamma_1\tilde{V}_1 + \gamma_2\tilde{V}_2)\cos\theta$. Here $\tilde{V}_i$ is the dimensionless settling velocity of the sediment size group i and γ_i is the fractional volume of this sediment group. Note that by definition $\gamma_1 + \gamma_2 = 1$.

In this study we focus on the underlying interaction of a polydisperse suspension and turbulence in planar turbidity currents. In particular, we focus on turbidity currents through submarine canyons on the continental slopes. In this scenario the flow is assumed to be planar and confined inside the canyon. Furthermore, the submarine canyon is assumed to be straight with a constant width. We further simplify some of the complex physics like resuspension, bed load transport and coupling with the bed topography by considering the turbidity current to be in auto-suspension mode (Bagnold, 1962; Sequeiros et al., 2009) propagating on an inclined flat bed. We restrict our attention to the body of the current and examine the effect of polydispersity on flow turbulence. Under these assumptions the total sediment load is conserved and the flow will reach a statistically steady state and as a consequence direct comparison of turbulence statistics of turbidity currents that have the same sediment load but differ in composition of their suspension can be made.

In this study we characterize the polydisperse suspension with a probability distribution of sediment size where different sediment sizes are parameterized in terms of their settling velocity $\tilde{V}$. Furthermore, the probability distribution is the fractional volume $\gamma(\tilde{V})$ occupied by the different sediment sizes in suspension and satisfies $\int_0^\infty \gamma(\tilde{V})\, d\tilde{V} = 1$. With this mathematical definition, we show that the parametric grouping that captures the damping of turbulent kinetic energy to be $Ri_\tau \tilde{V}_e \cos(\theta)$, where $\tilde{V}_e$ is the effective settling velocity of the polydisperse suspension. Furthermore, we demonstrate that the parametric grouping, $Ri_\tau \tilde{V}_e \cos(\theta)$, provides an accurate measure of the collective effect of a polydisperse suspension on flow turbulence. In particular, we observe the turbulent velocity statistics within a mono-, bi- or polydisperse turbidity current to be nearly the same, as long as the total amount of sediment and $Ri_\tau \tilde{V}_e \cos(\theta)$ are the same. The differences in the sediment size distribution between the different polydisperse currents only play a secondary role. As a consequence, a polydisperse suspension can be efficiently modeled as an equivalent monodisperse suspension whose sediment settling velocity is set equal to the effective settling velocity ($\tilde{V}_e$) of the polydisperse suspension.

It should be pointed out that an equivalent monodisperse suspension with a constant effective settling velocity over the entire domain will not accurately reproduce the mean sediment concentration or higher order sediment concentration statistics. This is because the vertical variation of sediment concentration and its associated higher order statistics in a polydisperse system strongly depends on the local sediment size distribution. So, it appears that turbulent velocity statistics is most influenced by depth-averaged global sediment size distribution and the net amount of sediment in suspension and not so much by the detailed distribution of sediment sizes in the vertical direction. Interestingly, by considering an equivalent monodisperse suspension with a depth-dependent effective settling velocity, we observe that it is possible to approximate both the velocity and sediment concentration statistics of the corresponding polydisperse suspension.

The equivalence between polydisperse and monodisperse currents to be established below is specific to turbulent turbidity currents. These observations and conclusions would be useful to build improved mathematical models of turbidity currents and better turbulence closures. By quantifying the details of interaction of polydisperse suspensions and turbulence in terms of global parametric quantities (total sediment load and effective settling velocity) will facilitate better interpretation and comparison of different experiments and field observations.

The problem of interaction of stratified scalar fields like temperature or concentration of passive species like salinity and turbulence is related to the interaction of stratified polydisperse suspension and turbulence in a turbidity current. The important distinguishing factor between the two problems is that the suspension in turbidity currents behaves as an active scalar which will not advect with the local fluid velocity. There has been a lot of work in the former field where turbulence damping and eventual relaminarization under varying extent of stratification has been investigated (Armenio and Sarkar, 2002; Taylor et al., 2005; Zonta, 2013; Zonta et al., 2012; Zonta and Soldati, 2013). Similarly, Cantero et al. (2012b) and Shringarpure et al. (2012) investigated the dynamics of turbulence suppression due to sediment stratification in turbidity currents. It remains to be further studied if dynamics of turbulence suppression and the equivalence between different suspensions can be extended to other polydisperse multiphase flows.

In Section 2 we will describe briefly a general mathematical formulation of polydisperse sediment suspensions. Section 3 discusses the underlying assumptions for a turbidity current and resulting simplified governing equations to be solved in this study. Section 4 presents the results from 14 different simulations that range from monodisperse, to polydisperse cases followed by a

Please cite this article as: M. Shringarpure et al., Equivalence of turbulence statistics between monodisperse and polydisperse turbidity currents, Advances in Water Resources (2017), http://dx.doi.org/10.1016/j.advwatres.2017.05.015

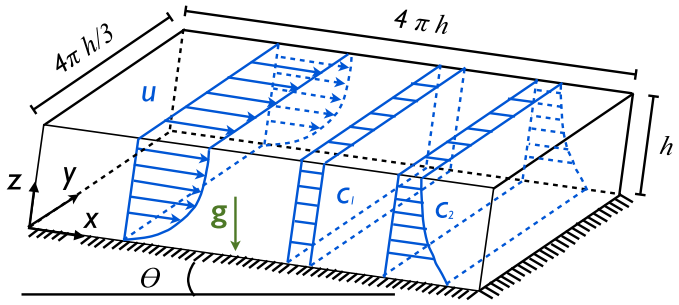

Fig. 1. Schematic of model geometry and set up. The figure shows a suspension made up of two sediment sizes whose concentration profiles in bed normal(z) direction are C_1 and C_2.

discussion of the results. In Section 5 simulation of equivalent monodisperse suspension with depth-dependent settling velocity is considered. Finally in Section 6 conclusions are drawn.

2. Problem formulation

A fully resolved simulation of a turbidity current with billions of particles in suspension is impractical, if not impossible. Typically for the flow regimes of interest, the response time of the sediment particles is smaller than the Kolmogorov time scale, which suggests that an Eulerian description of dispersed phase is well suited (Balachandar and Eaton, 2010). However, there are other complications associated with the Eulerian description. The main difficultly is that the suspended particles are characterized by multiple independent attributes like shape, size and material property which control their interaction with the surrounding continuous medium. Furthermore, in real suspensions these attributes can take wide range of values and as a result such suspensions need to be described by a multi-variate distribution function. In this section we will consider, as an example, a bivariate distribution where the two independent attributes are the sediment size D and the sediment density measured in terms of sediment-to-water density ratio $R = (\rho_s - \rho_w)/\rho_w$. Here ρ_s is the density of the sediment and ρ_w is the density of the ambient water. To study the spatial and temporal evolution of a suspension, a Population Balance Equation (PBE) (Ramkrishna, 2000) is typically solved. The PBE evolves the distribution function in space and time based on prescribed interactions like particle aggregation and breakage.

Here we consider the body of a turbidity current modeled as sediment-laden inclined periodic open channel flow (Cantero et al., 2009a, see TCR model in). Fig. 1 shows a schematic of the model geometry. As in turbidity currents, the flow in the proposed model is driven by the excess density imposed by the polydisperse suspension of sediment. We assume that the suspension is dilute and as a consequence the flow rheology is taken to be Newtonian and particle collisions are unimportant. This also allows the use of Boussinesq approximation. The distribution representing the sediment suspension is the bivariate volumetric concentration $c(\underline{\mathbf{x}}, t; D, R)$. Therefore the effect of polydisperse suspension leads to a mixture density

$$\rho_{mix}(\underline{\mathbf{x}}, t) = \rho_w\left[1 + \int_R\int_D R\, c(\underline{\mathbf{x}}, t; D, R)\, dD\, dR\right]. \tag{1}$$

The governing equations for this flow are

$$\frac{\partial u_i}{\partial t} + u_j\frac{\partial u_i}{\partial x_j} = -\frac{1}{\rho_w}\frac{\partial p}{\partial x_i} + \nu\frac{\partial^2 u_i}{\partial x_j\partial x_j} + g_i\int_R\int_D R\, c\, dD\, dR\,, \tag{2}$$

$$\frac{\partial u_i}{\partial x_i} = 0\,, \tag{3}$$

$$\frac{\partial c}{\partial t} + \frac{\partial}{\partial x_i}\Big[(v_i|D,R)c\Big] - \frac{\partial}{\partial x_i}\left(\mathcal{D}_{ij}\frac{\partial c}{\partial x_j}\right) = S(c), \tag{4}$$

where we have dropped the explicit dependence of the volumetric concentration to simplify notation. In the above indices $i = 1 \ldots 3$ and $j = 1 \ldots 3$ represent the three co-ordinate directions (x, y, z). Note that we use 1, 2, 3 and x, y, z interchangeably. Here (4) is the PBE (Marchisio and Fox, 2005; Ramkrishna, 2000), u_i is the fluid velocity, p is the pressure, ν is the kinematic viscosity, g_i the ith component of gravity, $\mathcal{D}_{ij}$ is the diffusivity tensor of sediment particles, and $S(c)$ is a source term accounting for accounting for coalescence, flocculation and breakage of sediment particles. It is typically an empirical closure that approximated the microscale physics of the polydisperse suspension. In (4), $(v_i|D, R)$ is the velocity of the sediment particles conditioned on the properties D and R. Also, the sediment volume fraction is small which means that fluid velocity can be considered to be solenoidal (Cantero et al., 2008a; Ferry and Balachandar, 2001). For the fluid velocity a no-slip boundary condition is enforced on the bottom boundary and a free-slip is enforced for the top boundary. For sediment concentration zero net concentration flux conditions are enforced at both boundaries. Mathematically, it can be written as

$$(v_z|D,R)\, c = \mathcal{D}_{iz}\frac{\partial c}{\partial z}. \tag{5}$$

Periodic boundary conditions are enforced in the streamwise and spanwise directions for all variables.

2.1. Stationary state mean flow equations

Mean flow equations averaged over turbulence can be obtained by substituting Reynolds decomposition $u_i = \langle u_i\rangle + u_i'$ and $c(\underline{\mathbf{x}}, t; D, R) = \langle c\rangle(z; D, R) + c'(\underline{\mathbf{x}}, t; D, R)$ in (2)–(4). Here $<\cdot>$ means an ensemble average and $(\cdot)'$ is the corresponding fluctuation. Note that because of the periodic boundary conditions in the streamwise and spanwise directions and statistical stationarity, the ensemble average can be represented by an average over time and over the streamwise x and spanwise y directions. The ensemble averaged quantities are then only functions of the bed-normal z direction. The mean z-momentum equation reduces to

$$0 = -\frac{d\langle w'w'\rangle}{dz} - \frac{1}{\rho_w}\frac{d\langle p\rangle}{dz} + g_z\int_R\int_D R\langle c\rangle(z; D, R)\, dD\, dR. \tag{6}$$

Integrating this equation in z gives the mean pressure distribution

$$\langle p\rangle(x, z) = -\rho_w\langle w'w'\rangle + \rho_w g_z\int_0^z\int_R\int_D \langle c\rangle(z; D, R)\, dD\, dR\, dz' + \mathcal{P}(x). \tag{7}$$

$\mathcal{P}$ is the streamwise pressure function, which turns out to be zero as the flow is driven purely by the excess density due to suspended sediments. The mean $x-$momentum equation is

$$0 = -\frac{d\langle u'w'\rangle}{dz} + \nu\frac{d^2\langle u\rangle}{dz^2} + g_x\int_R\int_D R\langle c\rangle(z; D, R)\, dD\, dR. \tag{8}$$

We can integrate the above equation in the z direction from the bottom ($z_b = 0$) to the top ($z_t = h$) boundary to obtain

$$\nu\frac{d\langle u\rangle}{dz}|_{z_b} = g_x\int_0^h\int_R\int_D R\langle c\rangle(z; D, R)\, dD dR\, dz\,, \tag{9}$$

where a free-slip boundary condition has been enforced on the top wall. The friction velocity u^* is defined as

$$u_*^2 = \nu\frac{d\langle u\rangle}{dz}|_{z_b} = g_x\,(RC)^{(v)}\,h\,. \tag{10}$$

Please cite this article as: M. Shringarpure et al., Equivalence of turbulence statistics between monodisperse and polydisperse turbidity currents, Advances in Water Resources (2017), http://dx.doi.org/10.1016/j.advwatres.2017.05.015

Here

$$(RC)^{(v)} = \frac{1}{h}\int_0^h \int_R \int_D R\langle c\rangle dD\, dR\, dz\,, \tag{11}$$

$$C^{(v)} = \frac{1}{h}\int_0^h \int_R \int_D \langle c\rangle dD\, dR\, dz\,. \tag{12}$$

The fractional volume can be defined as

$$\gamma(D,R) = \frac{1}{hC^{(v)}}\int_0^h \langle c\rangle(z;D,R)\, dz, \tag{13}$$

and by definition it satisfies the constraint

$$\int_R \int_D \gamma(D,R) dD\, dR = 1. \tag{14}$$

3. Simplified multigroup formulation for turbidity currents

The mathematical formulation presented in the previous section is a general framework applicable for a broad class of polydisperse flows. For the modeling of the body of a turbidity current several simplifications can be made.

1. Sediment particles are assumed to have the same density, thus reducing the distribution to a monovariate form. Furthermore, we assume that there is no shape effects so that sediment size D has a one to one correspondence with the sediment settling velocity V. The formula by Dietrich (Garcia, 2008) can be used to relate settling velocity with sediment size:

$$V(D) = \sqrt{gRD}\exp\{-b_1 + b_2\ln(Re_p) - b_3[\ln(Re_p)]^2 - b_4[\ln(Re_p)]^3 + b_5[\ln(Re_p)]^4\} \tag{15}$$

where

$$Re_p = \frac{\sqrt{gRD}D}{\nu}, \tag{16}$$

and $b_1 = 2.891394$, $b_2 = 0.95296$, $b_3 = 0.056835$, $b_4 = 0.002892$, $b_5 = 0.000245$. Therefore we can switch to sediment settling velocity V as the internal co-ordinate of the distribution function - $c(\underline{\mathbf{x}}, t; V)$.
2. Particle coalescence, flocculation and breakage are unimportant, which means the source term $S(c) = 0$.
3. For this work we assume that the turbidity current in autosuspension mode meaning that there is zero net flux of sediments between the flow and the bed. Since deposition is exactly balanced by resuspension, the total amount of sediment within the computational domain is conserved yielding

$$\frac{\partial}{\partial t}\int_{\mathcal{V}}\int_V c\, dV\, d\mathcal{V} = 0\,, \tag{17}$$

where $\mathcal{V}$ is the volume of the current.
4. $\mathcal{D}_{ij}$ is the diffusivity tensor of the sediment based on its characteristic length scale D. However, it must be emphasized that the source of this diffusivity is not Brownian motion, which is negligible for the ($O(100\,\mu m)$) finite-size sediment particles under consideration. The diffusion process is due to fluctuations in number density of the sediment particles, which leads to long range hydrodynamic interactions mediated by the carrier fluid (Mucha and Brenner, 2003; Segre et al., 2001). To simplify the analysis we will assume that the diffusion coefficient is isotropic (i.e., $\mathcal{D}_{ij} = \mathcal{D}\,\delta_{ij}$, $i = 1\ ,\ldots\ 3$; $j = 1\ \ldots\ 3$) and independent of sediment size.
5. Solution of the population balance Eq. (33) can be quite expensive. Some of the methods for solving PBEs are Monte Carlo Methods, Quadrature Method of Moments (QMOM), Direct Quadrature Method of Moments (DQMOM) (Marchisio and Fox, 2005; Ramkrishna and Singh, 2014). Here we simplify the problem by discretizing the continuous spectrum of sediment size into finite number of size bins. Thus, we define

$$c_m = \int_{V_{m-1/2}}^{V_{m+1/2}} c\, dV \tag{18}$$

to be the volumetric concentration in the mth bin of sediment particles whose settling velocity varies around V_m. Thus the distribution function is approximated as $c(\underline{\mathbf{x}}, t; V) = \sum_{m=1}^{N} c_m(\underline{\mathbf{x}}, t; V_m)$. Substituting this in the PBE equation along with the above assumptions results in a scalar transport equation for each discrete sediment size.
6. An Equilibrium–Eulerian approximation (Cantero et al., 2008a; Ferry and Balachandar, 2001) can be employed for the conditioned advection velocity $(v_i|D)$ in (4) such that

$$(v_i|D) = u_i + V_{mi}; \quad i = 1\ \ldots\ 3, \tag{19}$$

where u_i is the fluid velocity. V_{mi} is the ith component of the settling velocity of the mth sediment bin, which can be expressed in terms of the still fluid settling velocity V_m as $(V_{mx}, V_{my}, V_{mz}) = V_m(\sin\theta, 0, -\cos\theta)$ where θ is the angle of the bed with the horizontal direction.

With these simplifications the dimensional equations for the multigroup model with N discrete sediment sizes becomes

$$\frac{\partial u_i}{\partial t} + u_j\frac{\partial u_i}{\partial x_j} = -\frac{1}{\rho_w}\frac{\partial p}{\partial x_i} + \nu\frac{\partial u_i}{\partial x_j\partial x_j} + g_i R\sum_{m=1}^{N} c_m \tag{20}$$

$$\frac{\partial u_i}{\partial x_i} = 0, \tag{21}$$

$$\frac{\partial c_m}{\partial t} + \frac{\partial}{\partial x_i}[(u_i + V_{mi})c_m] = \mathcal{D}\frac{\partial^2 c_m}{\partial x_i\partial x_i}. \tag{22}$$

In the above indices $i = 1\ \ldots\ 3$ and $j = 1\ \ldots\ 3$ represent the three co-ordinate directions and subscript m denotes a discrete sediment size and $m = 1, \ldots, N$. Note that (12) and (13) become

$$C^{(v)} = \frac{1}{h}\int_0^h \sum_{m=1}^{N}\langle c_m\rangle\, dz\,, \text{ and} \tag{23}$$

$$\gamma_m = \frac{1}{hC^{(v)}}\int_0^h \langle c_m\rangle\, dz\,, \tag{24}$$

with the constraint $\sum_{m=1}^{N}\gamma_m = 1$. The total concentration of sediment is $c_t = \sum_{m=1}^{N} c_m$.

The boundary conditions for the governing equations (20)–(22) are periodicity along the x and y directions for all variables, and for the z direction

$$u_i = 0 \quad \text{at} \quad z = 0, \tag{25}$$

$$\frac{\partial u}{\partial z} = 0\,,\ \frac{\partial v}{\partial z} = 0 \quad \text{and} \quad w = 0 \quad \text{at} \quad z = h, \tag{26}$$

$$-V_m c_m\cos\theta = \mathcal{D}\frac{\partial c_m}{\partial z} \quad \text{at} \quad z = 0 \text{ and } h. \tag{27}$$

The error associated with the multigroup approximation can be quantified by comparing the moments of actual and discrete representation of the sediment size distribution function. We would like to choose the discrete sediment sizes to be such that the first few moments of the continuous sediment distribution are exactly matched. Note that the objective here is to match the global moments, i.e. moments computed from global quantities defined over the entire spatial domain. It can be easily shown that with N discrete sediment sizes, one can approximate $2N - 1$ moments exactly

Please cite this article as: M. Shringarpure et al., Equivalence of turbulence statistics between monodisperse and polydisperse turbidity currents, Advances in Water Resources (2017), http://dx.doi.org/10.1016/j.advwatres.2017.05.015

(Ramkrishna, 2000). For our study, the moment matching relations between the continuous and discrete distributions can be written as shown below

$$V_e = \int_0^\infty V\,\gamma(V)\,dV = \sum_{m=1}^{N} V_m\,\gamma_m, \tag{28}$$

$$M_2 = \int_0^\infty V^2\,\gamma(V)\,dV = \sum_{m=1}^{N} V_m^2\,\gamma_m. \tag{29}$$

In the above, V_e is the first moment of the fractional volume distribution of the polydisperse suspension and represents an effective settling velocity of the entire spectrum of sediment sizes, while M_2 is the corresponding second moment. Note that the matching of the zeroth moment is trivially satisfied since

$$M_0 = \int_0^\infty \gamma(V)\,dV = \sum_{m=1}^{N} \gamma_m = 1. \tag{30}$$

The matching of the zeroth moment is replaced by matching the values of $C^{(v)}$ for both the continuous and multigroup problems.

3.1. Dimensionless multigroup equations and numerical model

We employ the channel height h as the length scale, friction velocity u^* as the velocity scale, the total volumetric concentration $C^{(v)}$ as the concentration scale, and $t_s = h/u_*$ as the time scale. These choices lead to the following dimensionless governing equations

$$\frac{\partial \tilde{u}_i}{\partial \tilde{t}} + \tilde{u}_j\frac{\partial \tilde{u}_i}{\partial \tilde{x}_j} = -\frac{\partial \tilde{p}}{\partial \tilde{x}_i} + \frac{1}{Re_\tau}\frac{\partial \tilde{u}_i}{\partial \tilde{x}_j\partial \tilde{x}_j} + \tilde{g}_i\sum_{m=1}^{N}\tilde{c}_m\,, \tag{31}$$

$$\frac{\partial \tilde{u}_i}{\partial \tilde{x}_i} = 0, \tag{32}$$

$$\frac{\partial \tilde{c}_m}{\partial \tilde{t}} + \frac{\partial}{\partial \tilde{x}_i}\left[\left(\tilde{u}_i + \tilde{V}_{m,i}\right)\tilde{c}_m\right] = \frac{1}{Re_\tau Sc}\frac{\partial^2 \tilde{c}}{\partial \tilde{x}_j\partial \tilde{x}_j}, \tag{33}$$

where indices $i = 1\ldots3$ and $j = 1\ldots3$ represent the three coordinate directions and dimensionless variable are denoted by $\tilde{(\cdot)}$ and

$$Re_\tau = \frac{u_* h}{\nu}, \quad Sc = \frac{\nu}{\mathcal{D}}, \quad \tilde{g}_i = \{1, 0, -Ri_\tau\}, \quad Ri_\tau = \frac{1}{\tan\theta}. \tag{34}$$

In the above Re_τ is the shear Reynolds number, Ri_τ is the bulk Richardson number based on friction velocity which reduces to $1/\tan(\theta)$ for the choice of scaling variables, and Sc is the Schmidt number.

The multigroup model Eqs. (31)–(33) are solved employing a dealiased pseduospectral code (Canuto et al., 1988). For all the flow variables Fourier expansions are employed in the horizontal directions tangential to the bed ($\tilde{x}$ and $\tilde{y}$ directions) and a Chebyshev expansion is used in the bed normal direction ($\tilde{z}$). A time split method is used to solve the momentum equation and the incompressibility condition. A low storage mixed third-order Runge-Kutta and Crank-Nicolson scheme is used for temporal discretization of advection and diffusion terms. This scheme is carried out in three stages with pressure correction at the end of each stage. Details on implementation of this scheme can be found in the work by Cortese and Balachandar (1995). The domain size is $(\tilde{L}_x, \tilde{L}_y, \tilde{L}_z) = (4\pi h, 4\pi h/3, 1)$ and grid resolution is $(N_x, N_y, N_z) = (96, 96, 97)$.

4. Results and discussion

The list of simulations performed in this study are given in Table 1. In all the simulations $Re_\tau = 180$, $Ri_\tau = 11.43$, $Sc = 1$ are held fixed while the composition of sediment suspension is changed. $Ri_\tau = 11.43$ corresponds to a slope of 5° which is a typical inclination of the ocean floor in the continental slope region (Pinet, 2006). Real turbidity currents have much higher Re_τ ($O(10^5)$) which are inaccessible for direct numerical simulations (DNS). Although our simulations are at lower Re_τ they exhibit mature turbulence and the results are of relevance to real turbidity currents (Cantero et al., 2012a; 2012b).

To study the effect of sediment size distribution on turbulence statistics in a systematic way, we use moments of the polydisperse suspension to compare different suspensions. Here we have grouped all suspensions into set A and set B. In both sets the total sediment load $C^{(v)}$ is the same (this is a consequence of Re_τ being fixed at 180, see (10) and (34)), but the first moment of the total sediment volumetric concentration ($\tilde{V}_e$, see (28)) is different. $\tilde{V}_e$ is fixed at 0.01 and 0.02 for all cases in set A and set B, respectively.

Keeping $\tilde{V}_e$ fixed within each set assures that the total damping of turbulent kinetic energy by suspended sediments is held constant. To see this clearly, we can write the turbulent kinetic energy (TKE) equation as

$$\tilde{P} - \tilde{\epsilon} + \tilde{T} + \frac{1}{Re_\tau}\frac{d^2\langle\tilde{k}\rangle}{d\tilde{z}^2} = \tilde{\mathcal{S}}\,, \tag{35}$$

where

$$\tilde{k} = \frac{1}{2}\left\langle\tilde{u}'^2 + \tilde{v}'^2 + \tilde{w}'^2\right\rangle, \quad \tilde{P} = -\left\langle\tilde{u}'\tilde{w}'\right\rangle\frac{d\langle\tilde{u}\rangle}{d\tilde{z}}, \quad \tilde{\epsilon} = \frac{1}{Re_\tau}\left\langle\frac{\partial \tilde{u}_i'}{\partial \tilde{x}_j}\frac{\partial \tilde{u}_i'}{\partial \tilde{x}_j}\right\rangle, \tag{36}$$

$$\tilde{T} = -\frac{d}{d\tilde{z}}\left\langle\tilde{w}'\left(\frac{\tilde{u}'^2 + \tilde{v}'^2 + \tilde{w}'^2}{2} + \tilde{p}'\right)\right\rangle,$$
$$\tilde{\mathcal{S}} = -\sum_{m=1}^{N}\left\langle\tilde{u}'\tilde{c}_m'\right\rangle + Ri_\tau\sum_{m=1}^{N}\left\langle\tilde{w}'\tilde{c}_m'\right\rangle. \tag{37}$$

In the above, $\tilde{k}$ is TKE, $\tilde{P}$ is TKE production, $\tilde{\epsilon}$ is TKE dissipation, $\tilde{T}$ is TKE transport due to fluctuations in velocity and pressure, the last term on the left hand side of the equation is viscous transport of TKE and $\tilde{\mathcal{S}}$ is TKE damping due to suspended sediment. $\tilde{\mathcal{S}}$ can also be interpreted as the rate of TKE energy spent by the flow on suspended sediments. We can integrate (35) in the bed-normal direction to get the total TKE budget as

$$\tilde{\mathcal{P}} - \tilde{\mathcal{E}} + \frac{1}{Re_\tau}\left(\left[\frac{d<\tilde{k}>}{d\tilde{z}}\right]_0^1 - \frac{1}{Sc}\sum_{m=1}^{N}\left[\tilde{c}_m\right]_0^1\right) = \tilde{\beta} + Ri_\tau\tilde{V}_e\cos\theta \tag{38}$$

In the above,

$$\tilde{\mathcal{P}} = \int_0^1\tilde{P}\,d\tilde{z}, \qquad \tilde{\mathcal{E}} = \int_0^1\tilde{\epsilon}\,d\tilde{z}, \quad \text{and} \quad \tilde{\beta} = -\sum_{m=1}^{N}\int_0^1\left\langle\tilde{u}'\tilde{c}_m'\right\rangle d\tilde{z}. \tag{39}$$

Refer to Appendix A for the derivation. The two terms on the right hand side of (38) are the sediment induced damping terms. Previous DNS of turbidity currents driven by monodisperse (Shringarpure et al., 2012) and bidisperse suspension (Shringarpure et al., 2014) indicate that $\tilde{\beta}$ is proportional to the parametric grouping $\tilde{\mathcal{S}}_w^{(v)} = Ri_\tau\tilde{V}_e\cos\theta$, where $\tilde{\mathcal{S}}_w^{(v)}$ is a measure of total resuspension work rate. Therefore, the total TKE damping by suspended

Please cite this article as: M. Shringarpure et al., Equivalence of turbulence statistics between monodisperse and polydisperse turbidity currents, Advances in Water Resources (2017), http://dx.doi.org/10.1016/j.advwatres.2017.05.015

Table 1
List of simulations: γ_m refers to the volumetric fraction of sediment group m in the mixture and $\sum_{m=1}^{N}\gamma_m = 1$. $\tilde{V}_m$ refers to the settling velocity of sediment particles in the suspension. We fix $Re_\tau = 180$, $Ri_\tau = 11.42$ and $Sc = 1$ for all the simulations. In set A $\tilde{V}_e = \sum_{m=1}^{N}\gamma_m\tilde{V}_m = 0.01$ and in set B $\tilde{V}_e = \sum_{m=1}^{N}\gamma_m\tilde{V}_m = 0.02$. Not listed here is case 8. Case 8 corresponds to a simulation with monodisperse suspension with depth-varying settling velocity in the channel, fixed in time, and prescribed at initialization. This prescribed settling velocity for case 8 is the effective settling velocity computed from the stationary state of case 7B (see (49)).

case	$\tilde{V}_1$	γ_1	$\tilde{V}_2$	γ_2	$\tilde{V}_3$	γ_3	$\tilde{V}_4$	γ_4	$\tilde{M}_2$ (10^{-4})
1A	0.010	1.0	–	–	–	–	–	–	1.00
2A	0.000	0.8	0.05	0.2	–	–	–	–	5.00
3A	0.001	0.6250	0.0250	0.3750	–	–	–	–	2.35
4A	0.001	0.7692	0.04	0.2308	–	–	–	–	3.70
5A	0.005	0.8571	0.04	0.1429	–	–	–	–	2.50
6A	0.001	0.6875	0.025	0.2125	0.04	0.1000	–	–	2.94
7A	0.001	0.5500	0.005	0.3000	0.05	0.1300	0.0725	0.02	4.38
1B	0.020	1.0	–	–	–	–	–	–	4.00
2B	0.000	0.6	0.05	0.4	–	–	–	–	10.00
3B	0.010	0.6667	0.04	0.3333	–	–	–	–	6.00
4B	0.001	0.5128	0.04	0.4872	–	–	–	–	7.80
5B	0.002	0.6250	0.05	0.3750	–	–	–	–	9.40
6B	0.001	0.6154	0.04	0.2846	0.08	0.1000	–	–	11.00
7B	0.003	0.5000	0.02	0.1500	0.03	0.2500	0.08	0.1000	9.30

sediments is then $(1+\alpha)\tilde{\mathcal{S}}_w^{(v)}$, where $\alpha = \tilde{\beta}/\tilde{\mathcal{S}}_w^{(v)}$. This clearly shows that the overall TKE damping is proportional to the effective settling velocity of a polydisperse suspension. For a monodisperse suspension, the parameter reduces to $\tilde{\mathcal{S}}_w^{(v)} = Ri_\tau\tilde{V}\cos\theta$, which is the same as that considered in Cantero et al. (2012b) and Shringarpure et al. (2012). Although, this analysis shows that the total TKE damping may depend only on $\tilde{\mathcal{S}}_w^{(v)}$, we can anticipate the detailed turbulence statistics to additionally depend on the vertical distribution of sediments of different sizes. The simulations performed in this study explores this aspect in detail to address to what extent $\tilde{\mathcal{S}}_w^{(v)}$ is able to predict the collective effect of a polydisperse suspension on turbulence.

In both sets of simulations listed in Table 1, case 1 is the monodisperse suspension. Case 1A with $\tilde{V} = 0.01$ and case 1B with $\tilde{V} = 0.02$. In each set, we will refer to the monodisperse case (case 1) as the reference and compare other cases against it. Cases 2 to 5 are bidisperse suspensions. Case 6 in both the sets corresponds to a suspension made up of three sediment sizes, while case 7 corresponds to a suspension made up of four sediment sizes. In case 7, the settling velocity of the largest sediment particles is about 8 times larger than the monodisperse case. In all the multi-sized suspensions the settling velocity of the largest sediment size is about 30 to 80 times the smallest sediment size. Refer to Table 1 for complete details.

The maximum sediment size or the settling velocity can be chosen to be arbitrarily high. However, such choices would be incompatible on two fronts. First, sediment particles can be held in suspension only if their settling velocity is less than the *rms* vertical velocity fluctuations in the flow (Middleton, 1976). Recent work (Salinas et al., 2017) shows that sediment particles whose $\tilde{V} > 0.1$, typically, get sequestered very close to the bottom of the current. Second, the assumption that the turbidity current is in the autosuspension mode places an implicit restriction on the sediment size and choosing a large sediment size will violate this assumption. In other words, these sediments should be sufficiently small so that there is no net flux to the bed, but they should be sufficiently large to stratify in the bed normal direction. Such sediment sizes are classified as coarse wash load (Garcia, 2008).

Although the different cases in sets A and B have the same total volumetric concentration of sediment and same effective settling velocity, their higher order moments are quite different. To highlight this difference, Table 1 lists the second moment $\tilde{M}_2$ for all the cases. All the simulations are initialized with uniform distribution of constituent sediment sizes and after an initial transient phase, turbulence statistics associated with the stationary state are accumulated. Various turbulence statistics like the mean sediment concentration, mean streamwise velocity, *rms* velocity profiles, Reynolds stress, Reynolds flux and TKE production, dissipation and damping are gathered and compared.

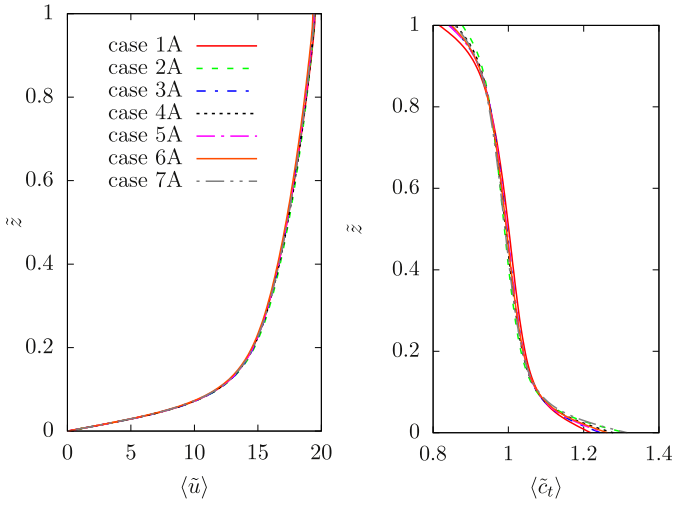

Fig. 2. Profiles of mean streamwise velocity $\langle\tilde{u}\rangle$ and total mean sediment concentration $\langle\tilde{c}_t\rangle$ for all cases in set A.

4.1. Mean streamwise velocity and sediment concentration

Figs. 2a and 3 a show the mean streamwise velocity profiles for all cases in set A and set B respectively. The profiles nearly fall on top of each other and on the reference profile of the monodisperse case 1. The extent of deviation of the velocity profiles of cases 2 to 7 from that of case 1 is quantified by the L2 norm of the difference and presented in Tables 2 and 3. Note that these L2 norms are normalized by the reference case 1 and computed as follows

$$||\langle\cdot\rangle||_2 = \frac{\int_0^1 \left(\langle\cdot\rangle - \langle\cdot\rangle_{ref}\right)^2 d\tilde{z}}{\int_0^1 \langle\cdot\rangle_{ref}^2 d\tilde{z}}. \tag{40}$$

The L2 difference of mean streamwise velocity for the different cases is observed to be $O(10^{-5})$.

Please cite this article as: M. Shringarpure et al., Equivalence of turbulence statistics between monodisperse and polydisperse turbidity currents, Advances in Water Resources (2017), http://dx.doi.org/10.1016/j.advwatres.2017.05.015

Table 2
L2 norms of difference in various turbulence statistics computed for set A from the monodisperse case. $\tilde{S}$ represents the TKE damping terms (see right hand side of (35)). Refer to (40) for the exact mathematical form of the L2 norm reported here.

case	$\|\|\langle\tilde{u}\rangle\|\|_2$ (10^{-5})	$\|\|\langle\tilde{c}\rangle_t\|\|_2$ (10^{-3})	$\|\|\tilde{u}_{rms}\|\|_2$ (10^{-4})	$\|\|\tilde{w}_{rms}\|\|_2$ (10^{-4})	$\|\|\tilde{\nu}_{rms}\|\|_2$ (10^{-4})	$\|\|\langle\tilde{u}'\tilde{w}'\rangle\|\|_2$ (10^{-4})	$\|\|\langle\tilde{w}'\tilde{c}_t'\rangle\|\|_2$ (10^{-3})	$\|\|\tilde{P}\|\|_2$ (10^{-4})	$\|\|\tilde{\epsilon}\|\|_2$ (10^{-4})	$\|\|\tilde{S}\|\|_2$ (10^{-3})
2A	2.8444	4.4842	1.2656	0.2713	0.9706	1.3079	17.876	2.7880	0.8085	1.1073
3A	1.0354	3.9917	2.5305	0.2914	1.0822	0.2366	1.9636	1.0806	1.1077	1.1364
4A	0.4317	4.7243	1.4700	0.1394	0.5101	0.7022	8.7817	1.8719	0.8922	1.2941
5A	0.6418	4.6650	0.4993	0.7053	0.2072	3.1423	2.7063	6.4000	5.6207	1.3223
6A	4.5558	4.7751	1.5625	2.1248	1.0865	7.7010	4.5398	18.186	14.970	1.3907
7A	0.4997	5.4423	0.9157	1.5198	0.9157	4.3601	13.647	8.5274	5.1111	1.2693

Table 3
L2 norms of difference in various turbulence statistics computed for set B from the monodisperse case. $\tilde{S}$ represents the TKE damping terms (see right hand side of (35)) Refer to (40) for the exact mathematical form of the L2 norm reported here.

case	$\|\|\langle\tilde{u}\rangle\|\|_2$ (10^{-4})	$\|\|\langle\tilde{c}\rangle_t\|\|_2$ (10^{-2})	$\|\|\tilde{u}_{rms}\|\|_2$ (10^{-4})	$\|\|\tilde{w}_{rms}\|\|_2$ (10^{-4})	$\|\|\tilde{\nu}_{rms}\|\|_2$ (10^{-4})	$\|\|\langle\tilde{u}'\tilde{w}'\rangle\|\|_2$ (10^{-4})	$\|\|\langle\tilde{w}'\tilde{c}_t'\rangle\|\|_2$ (10^{-3})	$\|\|\tilde{P}\|\|_2$ (10^{-4})	$\|\|\tilde{\epsilon}\|\|_2$ (10^{-4})	$\|\|\tilde{S}\|\|_2$ (10^{-3})
2B	2.2183	3.0364	2.2587	1.2204	1.1157	5.6759	11.531	5.5690	1.6932	2.0087
3B	0.2498	1.3696	0.7736	0.1668	0.2051	0.9314	1.4046	1.6305	0.4915	1.2318
4B	1.0854	3.0324	3.6762	0.5164	0.5218	2.2982	4.8423	2.8445	0.6769	2.3014
5B	1.3586	3.0363	4.2819	1.6250	2.0224	5.2225	9.2998	6.6835	1.5044	2.8312
6B	0.7366	3.2395	16.340	3.1493	2.8236	12.260	15.594	22.169	7.1280	4.3496
7B	0.7434	3.0097	2.3646	1.2483	2.2841	3.3861	8.7869	2.4291	1.1645	4.0141

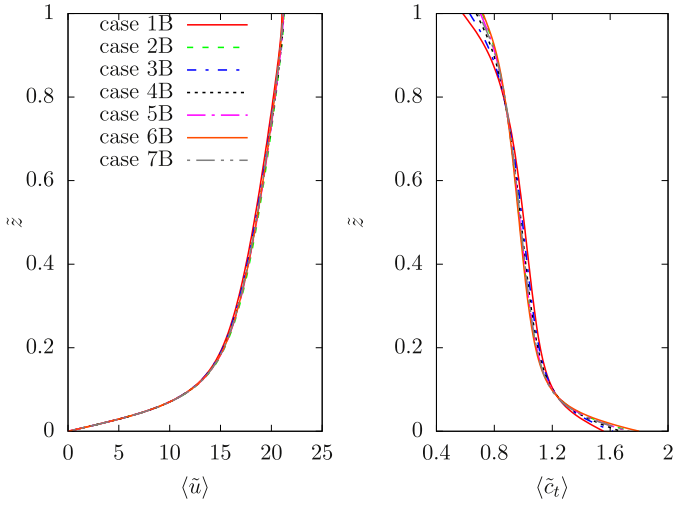

Fig. 3. Profiles of mean streamwise velocity $\langle\tilde{u}\rangle$ and total mean sediment concentration $\langle\tilde{c}_t\rangle$ for all cases in set B.

Figs. 2b and 3b show vertical variation of mean total sediment concentration $\langle\tilde{c}_t\rangle$ for all the cases in set A and set B. The mean total sediment concentration is the local excess density or the driving force imposed by suspended sediments. Unlike the mean streamwise velocity profiles, the mean total concentration profiles do not completely collapse onto the reference profile of case 1. Substantial differences are seen near the top and bottom boundaries. Away from the boundaries the concentration gradients are similar but the profiles are slightly shifted below the reference profile of case 1. A closer examination shows that these differences from the reference case increases with the increasing value of the second moment $\tilde{M}_2$ (see Table 1). For the reference case $\tilde{M}_2 = 1$ and with increasing $\tilde{M}_2$ we observe a slight but noticeable reduction in the mean total sediment concentration in the interior of the domain. Such deviations are to be expected when a polydisperse suspension is compared with an equivalent monodisperse suspension. It is straightforward to see that some of the sediment sizes of the polydisperse suspension will settle faster than the effective settling velocity, while some other sizes will settle slower and as a result, there will be increased accumulation of finer sediments near the top and coarser sediments towards the bottom with a net reduction in concentration in the middle for a polydisperse case. A simple measure of this spread in settling velocity can be written as

$$\int_0^1 \int_{\tilde{V}} (\tilde{V} - \tilde{V}_e)^2 \langle\tilde{c}\rangle d\tilde{V} d\tilde{z} = \tilde{M}_2 - \tilde{V}_e^2 \,, \tag{41}$$

and thus explaining the observed dependence on $\tilde{M}_2$.

The interesting feature of this result is that even though the vertical distribution of local driving force represented by the mean total sediment concentration varies somewhat between the different cases, the mean streamwise velocity which is the mean response to the driving force tends to collapse on to the reference profile. This insensitivity to the vertical distribution of the driving force is only when the flow is turbulent. In Section 4.3 we will look at the laminar solution of the governing equations and highlight key difference caused by the existence of turbulence. The L2 norm of the difference in the total concentration profiles of the different cases are given in Tables 2 and 3. As expected, the L2 norm of the differences, although still small, are 2 orders of magnitude higher than those for streamwise velocity profiles.

The total sediment settling flux is defined as the sum of the sediment fluxes of the N different sediment sizes (i.e., $\sum_{m=1}^{N} \tilde{V}_{mz}\langle\tilde{c}_m\rangle$) and its vertical variation for all cases in set A and set B is shown in Fig. 4. Unlike the mean velocity profiles, noticeable differences between the different cases within a set can be observed. Mathematically, the sediment settling flux is the first moment of local distribution of polydisperse sediment suspension in the flow. When averaged over the vertical direction yields

$$\int_0^1 \sum_{m=1}^{N} \tilde{V}_{mz}\langle\tilde{c}_m\rangle d\tilde{z} = \sum_{m=1}^{N} \tilde{V}_{mz}\gamma_m = \tilde{V}_e \,. \tag{42}$$

It can be seen from the figures that in all the cases the depth averaged sediment settling flux is equal to 0.01 and 0.02 in sets A and B, respectively. Again a systematic increasing departure from the reference case with increasing second moment $\tilde{M}_2$ can also be observed. Therefore these profiles demonstrate that even though the effective settling velocity $\tilde{V}_e$ matches for all the cases, the local behavior (as a function of $\tilde{z}$) can be quite different.

In turbidity currents, sediment particles are held in suspension through a balance between the downward settling flux and an upward turbulent flux, and this balance is established for every sediment group. Adding over all the sediment groups, the net

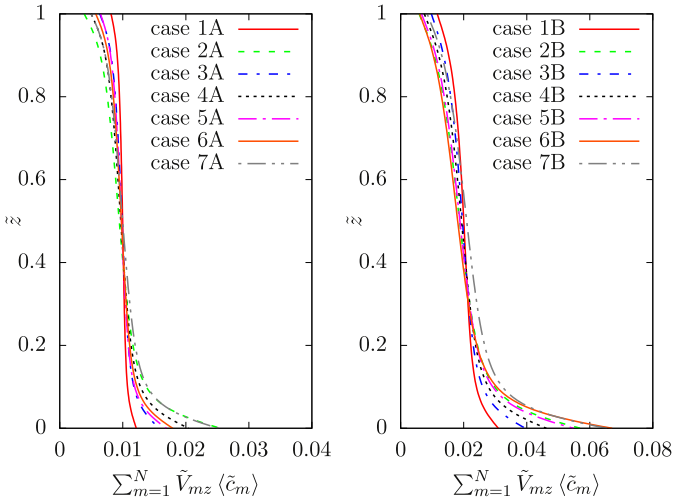

Fig. 4. Profiles of total sediment settling flux for all cases in set A and set B.

balance at a given vertical location within the channel can be written as

$$\sum_{m=1}^{N} \tilde{V}_{mz} \langle \tilde{c}_m \rangle - \left\langle \tilde{w}' \sum_{m=1}^{N} \tilde{c}'_m \right\rangle = 0. \tag{43}$$

Note that this relation is valid for a statistically stationary state and away from the top and bottom boundaries where the diffusive flux is negligible. Since we observed that the settling flux profiles differ greatly, we expect that the Reynolds flux profiles will also show noticeable differences between the different cases. Similar differences can be expected in other higher order statistics as well, which will be explored below.

4.2. Higher order turbulence statistics

Here we will present the results for set A only as all the observations and associated conclusions from the results of set A extend to set B. Refer to Appendix C for all the corresponding figures showing statistics obtained from cases in set B. Fig. 5 show $\tilde{u}_{rms}$, $\tilde{v}_{rms}$ and $\tilde{w}_{rms}$ profiles for all the cases in set A. Profiles of all three quantities for all the cases collapse onto the reference profile of case 1. The L2 norm of the difference in the *rms* profiles for different cases are listed in Table 2. Like the mean streamwise velocity profiles, the L2 norm of the difference is quite low at $O(10^{-4})$ of the reference monodisperse case. Fig. 6 show the Reynolds stress $-\langle \tilde{u}'\tilde{w}' \rangle$ and Reynolds flux $\sum_{m=1}^{N} \langle \tilde{w}'\tilde{c}'_m \rangle$ profiles for all cases in set A. While good collapse is observed for Reynolds stress, Reynolds flux profiles differ substantially, which is in agreement with the behavior observed in Fig. 4.

Profiles of TKE production and dissipation for the different cases show a good collapse onto the corresponding reference profile of case 1 (see Fig. 7). It is expected that TKE damping due to sediment suspension will depend on sediment size distribution as it is a function of Reynolds flux ($\langle \tilde{w}'\tilde{c}'_t \rangle$) which was shown to have substantial dependence. From the figures it is clear that the turbulence statistics, which are not associated with sediment concentration, of all cases collapse onto a unique profile suggesting that the statistics are nearly independent of the sediment size distribution. In other words, the zeroth and first moments of fractional sediment volume distribution are the most important factors that control the turbulent velocity field. As a consequence, it is possible to approximate a complicated polydisperse suspension by a monodisperse suspension whose sediment size has a settling velocity of $\tilde{V}_e$. However, it is important to emphasize that this simplification

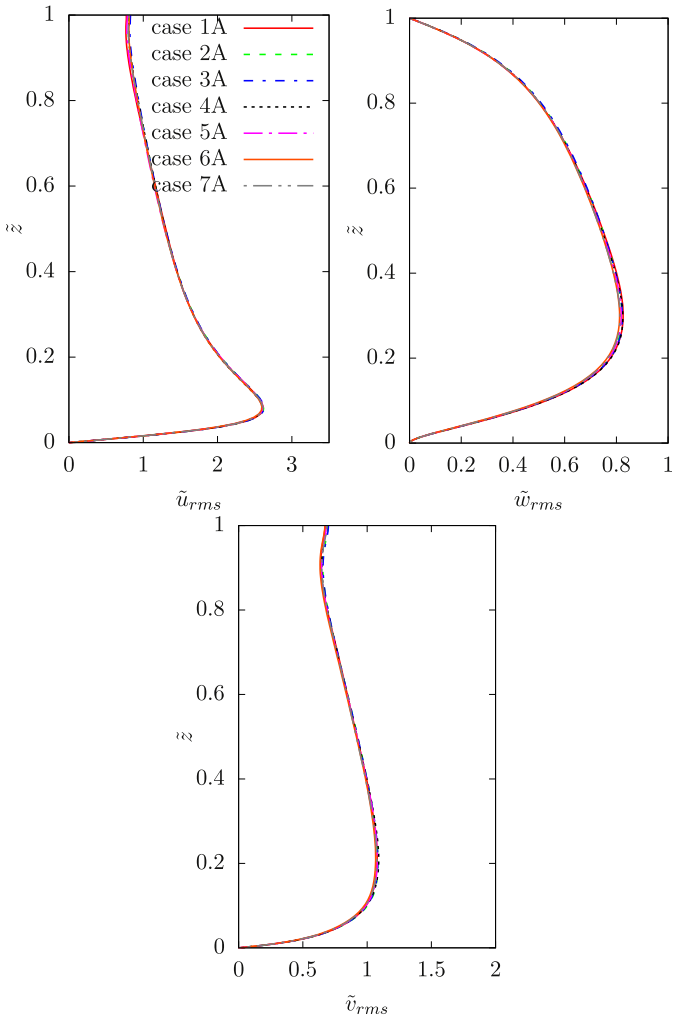

Fig. 5. Profiles of streamwise ($\tilde{u}_{rms}$), spanwise($\tilde{v}_{rms}$) and wall normal ($\tilde{w}_{rms}$) *rms* velocity for all cases in set A.

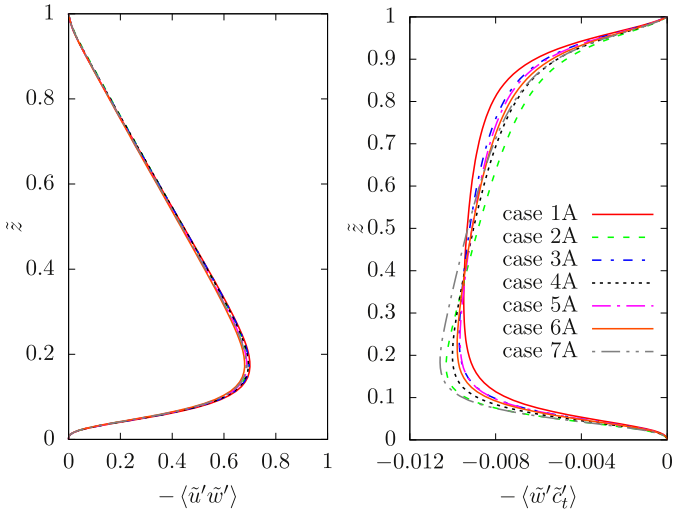

Fig. 6. Profiles of Reynolds stress $\langle \tilde{u}'\tilde{w}' \rangle$ and Reynolds flux $\langle \tilde{w}'\tilde{c}'_t \rangle$ for all cases in set A.

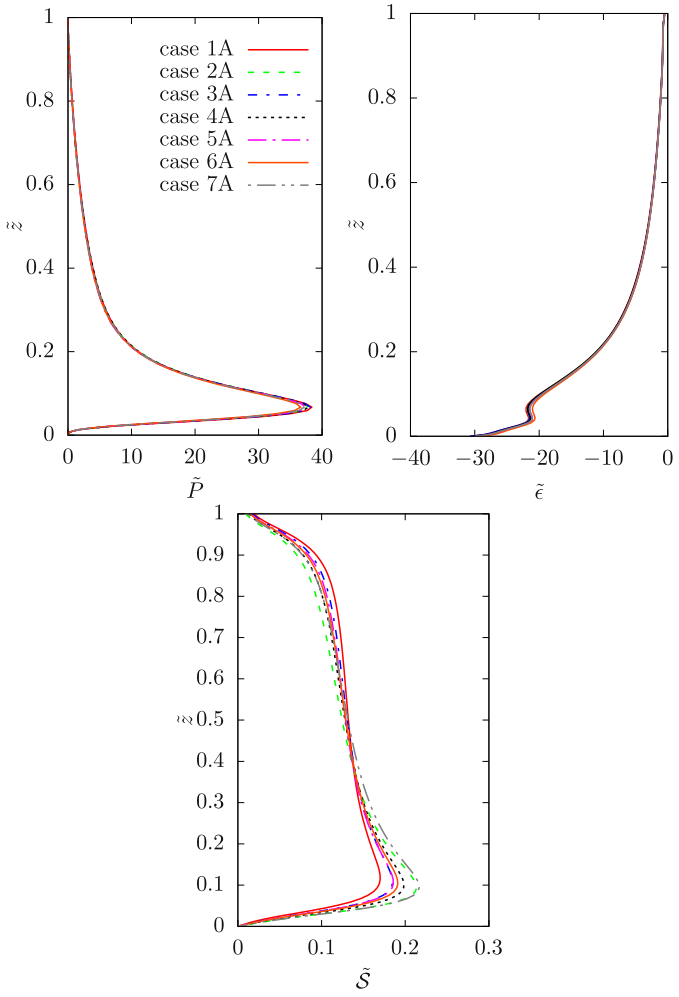

Fig. 7. Profiles of TKE production ($\tilde{P}$), TKE dissipation ($\tilde{\epsilon}$) and TKE damping ($\tilde{S}$) for all cases in set A.

has the important limitation that the flow statistics associated with sediment concentration will not be captured appropriately by the monodisperse suspension. We will address this in Section 5.

4.3. Laminar solution

Is the equivalence between polydisperse suspensions and its equivalent monodisperse suspension inherently embedded in mathematical model? Will this equivalence manifest across the range of Re_τ? Here we demonstrate that the approximate equivalence is restricted to only turbulent flow conditions. In other words such indifference of the velocity statistics to details of the driving potential requires strong turbulent mixing in the vertical direction. It can be shown that the observed equivalence breaks down when we consider laminar solution of the governing equation given in (31)–(33). The laminar solution for velocity and sediment concentration are given below (for derivation see Appendix B)

$$\tilde{c}_m = A_m \exp(Re_\tau\, Sc\, \tilde{V}_{mz}\, \tilde{z}), \tag{44}$$

$$\tilde{u} = -Re_\tau \sum_{m=1}^{N} \frac{A_m}{Re_\tau\, Sc\, \tilde{V}_{mz}} \left[\frac{\exp(Re_\tau\, Sc\, \tilde{V}_{mz}\, \tilde{z})}{Re_\tau\, Sc\, \tilde{V}_{mz}} - \tilde{z}\, \exp(Re_\tau\, Sc\, \tilde{V}_{mz}) - \frac{1}{Re_\tau\, Sc\, \tilde{V}_{mz}} \right]. \tag{45}$$

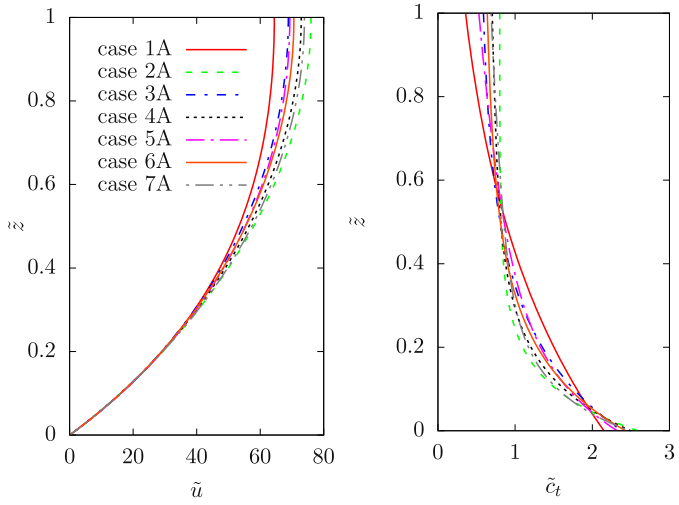

Fig. 8. Profiles of streamwise velocity $\tilde{u}$ and total sediment concentration $\tilde{c}_t$ obtained from the laminar solution of the governing equations for all cases in set A.

Table 4
L2 norms of laminar solution (velocity and total sediment concentration) for all cases in set A and set B. L2 norms of cases 2 to 7 represent the extent of deviation from the laminar solution of case 1. Refer to (40) for the exact mathematical form of the L2 norm reported here.

case	$\|\|\tilde{u}\|\|_2$ (10^{-2})	$\|\|\tilde{c}_t\|\|_2$ (10^{-2})
2A	1.7780	6.1239
3A	0.2249	1.3210
4A	0.9262	3.5856
5A	0.3228	1.0881
6A	0.4693	2.1382
7A	1.2351	3.8416
2B	7.5885	7.6402
3B	1.0846	1.0158
4B	3.6232	3.9234
5B	6.3448	6.1713
6B	7.8823	7.3312
7B	4.0966	3.6353

In the above,

$$A_m = \frac{\gamma_m Re_\tau\, Sc\, \tilde{V}_{mz}}{\exp(Re_\tau\, Sc\, \tilde{V}_{mz}) - 1}. \tag{46}$$

Fig. 8a show the laminar velocity profiles of all the cases of set A. Also, Fig. 8b show the total sediment concentration obtained from the laminar solution for each constituent sediment size present in the suspension of all the cases in set A. Comparing this figure with Fig. 2 (for the turbulent simulations), we can clearly see that the collapse of streamwise velocity is now absent and the deviation of total sediment concentration is much more pronounced in case of laminar solution. The deviation from the laminar solution of the equivalent monodisperse suspension is computed as the L2 norm of the difference for cases 2 to 7. For each case in set A, the L2 norm of the difference for the laminar solution is approximately 2 orders of magnitude larger than those of the corresponding turbulent flow. These results are tabulated in Table 4. This establishes that the laminar solution does not allow the same simplification of a polydisperse suspension observed in turbulent flows. Note that laminar velocity and total sediment concentration profiles of cases in set B are qualitatively similar to those of set A and all the above observations and conclusions presented here consistently extend to set B. Appendix C shows all the corresponding figures for set B.

Please cite this article as: M. Shringarpure et al., Equivalence of turbulence statistics between monodisperse and polydisperse turbidity currents, Advances in Water Resources (2017), http://dx.doi.org/10.1016/j.advwatres.2017.05.015

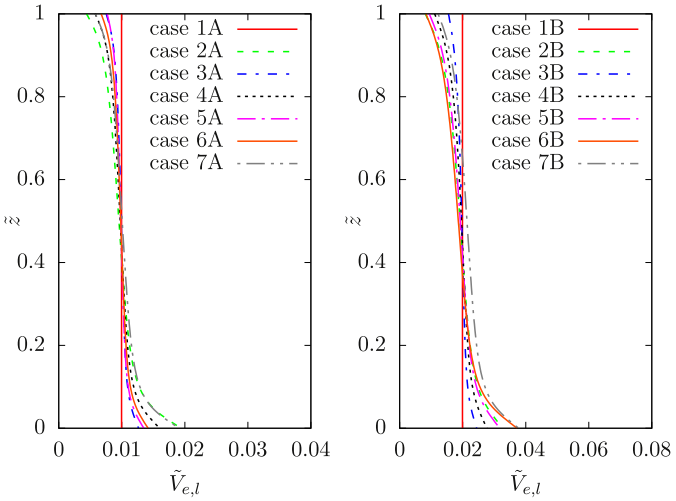

Fig. 9. Profiles of effective settling velocity $\tilde{V}_{e,l}$ all cases in set A and set B.

5. Depth-dependent effective settling velocity

The moments of continuous and discrete sediment distributions defined in Eqs. (28) and (29) are global quantities as they are based on depth averaged fractional volumes γ_m. Equivalently we can define depth-dependent moments of the local sediment distribution as

$$\tilde{M}_{0,l}(\tilde{z}) = \sum_{m=1}^{N} \langle \tilde{c} \rangle_m \tag{47}$$

$$\tilde{M}_{1,l}(\tilde{z}) = \sum_{m=1}^{N} \tilde{V}_{mz} \langle \tilde{c} \rangle_m. \tag{48}$$

From the above definition we obtain the zeroth moment to be the same as the normalized total sediment concentration $\langle \tilde{c}_t \rangle(\tilde{z})$. In all the simulations initially all constituent sediment sizes are uniformly distributed in the vertical direction with superimposed random perturbation, and consequently, at $t = 0$ we have $\tilde{M}_{0,l} = 1$ and $\tilde{M}_{1,l} = \tilde{V}_e$, which are the same as the global zeroth and first moments.

Once the simulations begin, the sediment particles settle down at their respective settling velocities and turbulence tends to mix them vertically. At the bottom boundary we enforce a resuspension flux through an effective diffusive process which ensures that total sediment load of each constituent sediment size is conserved. The overall effect of this evolution is that the depth-dependent moments which are based on local sediment concentration start deviating from the global moments and become a function of $\tilde{z}$. Each sediment size reaches its stationary state when its downward settling flux is balanced by the upward Reynolds flux (see (43)).

We can define the effective local settling velocity $\tilde{V}_{e,l}(\tilde{z})$ as

$$\tilde{V}_{e,l}(\tilde{z}) = \frac{\sum_{m=1}^{N} \tilde{V}_m \langle \tilde{c} \rangle_m}{\sum_{m=1}^{N} \langle \tilde{c} \rangle_m}. \tag{49}$$

This definition of effective local settling velocity along with local mean sediment concentration ensures perfect balance of net local sediment flux. Fig. 9 shows the profiles of effective local settling velocity $\tilde{V}_{e,l}$ for all cases in sets A and B. In cases 1A and 1B, $\tilde{V}_{e,l}$ is constant and is equal to 0.01 and 0.02, respectively. However, for all other cases, $\tilde{V}_{e,l}$ varies with height. Close to the bottom $\tilde{V}_{e,l}$ is closer to the settling velocity of the largest sediment, while near the top boundary, $\tilde{V}_{e,l}$ is closer to the settling velocity of the smallest sediment in the suspension. This captures the physical reality of the turbidity currents, i.e., in a turbidity current driven by polydisperse suspension we expect to find large sediments near the bottom of the flow, while the smaller sediments will be more common near the top.

From the perspective of an improved mathematical model, an ideal approximation of a polydisperse suspension with an equivalent monodisperse suspension is when the settling velocity of the monodisperse suspension varies with channel height as given by $\tilde{V}_{e,l}$. For a mondisperse suspension such a depth-dependent settling velocity has no direct physical meaning. However, it can serve as a mathematical model and an approximation for a more complex polydisperse system. With such a mathematical formulation, we want to examine if all turbulence statistics of the polydisperse suspension, including those involving sediment concentration, will be well captured by the monodisperse suspension.

5.1. Equivalent monodisperse suspension with depth-dependent settling velocity

In this section we will consider simulation of a monodisperse suspension with a depth-dependent settling velocity that will be referred to as $\tilde{V}_{mono}(\tilde{z})$. This depth-dependent settling velocity will be chosen to match the effective local settling velocity of a chosen polydisperse case given in (49). Note that the effective local settling velocity is known only through a direct numerical simulation of the polydisperse system, since the $\tilde{z}$-dependence of the mean concentration $\langle \tilde{c} \rangle_m$ of the different sediment sizes is not known a-priori. They are known only through an ensemble average of the simulation results in the statistically stationary state, only after the transient effects have fully decayed. Thus, the simulations with equivalent monodisperse to be described below is not of practical value, since it requires input from the polydisperse system that it will approximate. Our purpose is to see if a monodisperse system, with an ideal depth-dependent settling velocity, can approximate a polydisperse current. Here it must be pointed out that there are rigorously derived computational methods, such as QMOM and DQMOM (Marchisio and Fox (2005); Ramkrishna and Singh (2014)), proposed in the literature to solve the population balance equation. The present approach of an equivalent monodisperse suspension with depth-dependent settling velocity can be related to these approaches.

In the monodisperse simulation the depth-dependent settling velocity of the sediment will be held the same over time. The initial starting condition for the equivalent monodisperse suspension is a depth-independent uniform sediment concentration, which is the same as in all other simulations considered. The initial transient evolution of the monodisperse system is not expected to mimic the corresponding transient state of the polydisperse system very well. This discrepancy is due to the fact that the depth-dependent settling velocity used in the monodisperse system approximates only the stationary state of the polydisperse system. Thus, all comparisons between the equivalent monodisperse and polydisperse systems will be in the stationary regime.

Given these assumptions, we evaluate the effect of variable settling velocity on the governing equations and other important relations presented in the previous sections. The momentum equation will be unaffected as it does not directly depend on the sediment settling velocity (see (2), (31), (20)). The coupling between the flow and the sediment suspension is through the body force term which only depends on the sediment concentration. On the other hand sediment settling velocity directly controls the evolution of sediment concentration through the advection term in the concentration equation (see (33)). The TKE equation will also be

Please cite this article as: M. Shringarpure et al., Equivalence of turbulence statistics between monodisperse and polydisperse turbidity currents, Advances in Water Resources (2017), http://dx.doi.org/10.1016/j.advwatres.2017.05.015

Table 5
L2 norms of difference in various turbulence statistics computed for case 7B from the monodisperse with depth-varying settling velocity case (referred to as case 8). $\tilde{\mathcal{S}}$ represents the TKE damping terms (see right hand side of (35)) Refer to (40) for the exact mathematical form of the L2 norm reported here.

case	$\|\|\langle\tilde{u}\rangle\|\|_2$ (10^{-6})	$\|\|\langle\tilde{c}\rangle_t\|\|_2$ (10^{-6})	$\|\|\tilde{u}_{rms}\|\|_2$ (10^{-5})	$\|\|\tilde{w}_{rms}\|\|_2$ (10^{-5})	$\|\|\tilde{v}_{rms}\|\|_2$ (10^{-5})	$\|\|\langle\tilde{u}'\tilde{w}'\rangle\|\|_2$ (10^{-5})	$\|\|\langle\tilde{w}'\tilde{c}_t'\rangle\|\|_2$ (10^{-5})	$\|\|\tilde{P}\|\|_2$ (10^{-5})	$\|\|\tilde{\epsilon}\|\|_2$ (10^{-5})	$\|\|\tilde{\mathcal{S}}\|\|_2$ (10^{-5})
7B	1.8085	1.3928	8.2156	1.3684	2.3205	1.4533	5.3198	1.6198	2.0182	6.2539

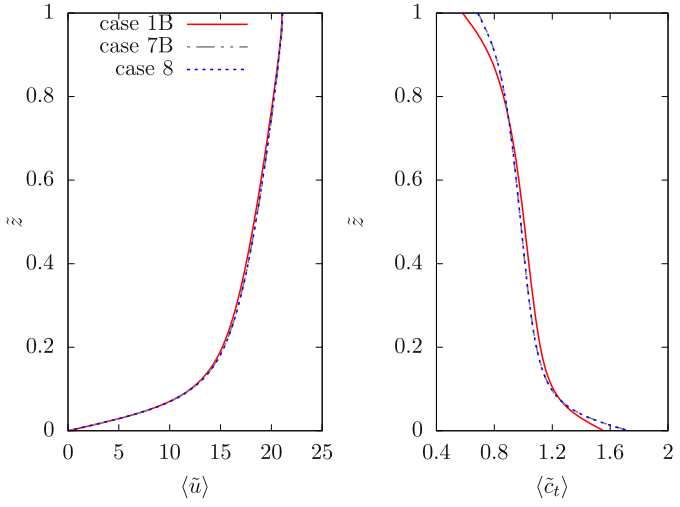

Fig. 10. Profiles of mean streamwise velocity $\langle\tilde{u}\rangle$ and total mean sediment concentration $\langle\tilde{c}_t\rangle$ for cases 1B, 7B and 8 (monodisperse suspension with variable settling velocity). We choose the settling velocity of the monodisperse suspension of case 8 inside the channel to be equal to the local effective settling velocity obtained for case 7B (see Fig. 9 and Eq. (49)).

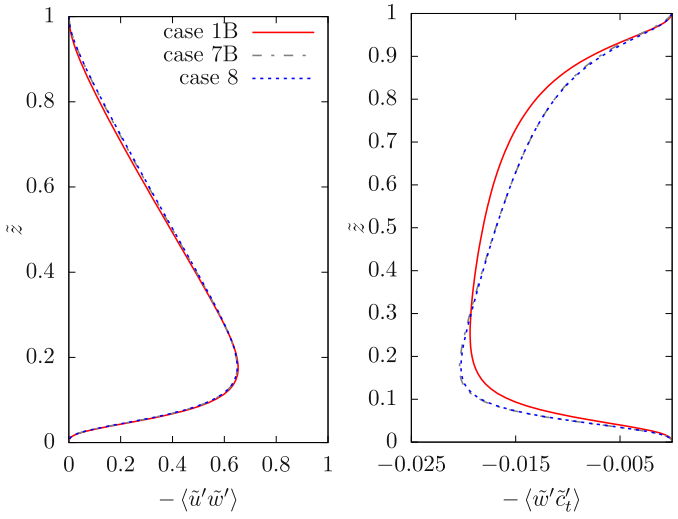

Fig. 11. Profiles of Reynolds stress $(\tilde{u}'\tilde{w}')$ and Reynolds flux $(\tilde{w}'\tilde{c}_t')$ for cases 1B, 7B and 8 (monodisperse suspension with variable settling velocity). We choose the settling velocity of the monodisperse suspension of case 8 inside the channel to be equal to the local effective settling velocity obtained for case 7B (see Fig. 9 and Eq. (49)).

modified and the modified form is as shown below

$$\tilde{\mathcal{P}} - \tilde{\mathcal{E}} + \frac{1}{Re_\tau}\left(\left[\frac{d<\tilde{k}>}{d\tilde{z}}\right]_0^1 - \frac{1}{Sc}[\langle\tilde{c}\rangle]_0^1\right) = \tilde{\beta} + Ri_\tau\left(\int_0^1 \tilde{V}_{mono}(\tilde{z})\langle\tilde{c}\rangle_{mono}d\tilde{z}\right)\cos\theta, \quad (50)$$

All the terms on the left hand side are the same as before (see (39)), while the damping term on the right hand side now accounts for the depth-dependent settling velocity.

Here we consider the polydisperse suspension case 7B with 4 constituent sediment sizes. Accordingly, we have assumed the depth-dependent settling velocity of the monodisperse suspension to be from the stationary state of case 7B (i.e., $\tilde{V}_{mono} = \tilde{V}_{e,l}^{(7B)}$). We refer to this monodisperse simulation with depth-dependent settling velocity as case 8. Fig. 10 shows the mean streamwise velocity and mean sediment concentration of cases 1B, 7B and 8. The enforced local settling velocity in case 8 dictates the evolution of sediment within the channel and the concentration profiles of case 7B and 8 are almost on top of each other. Similarly we expect better agreement between various higher order statistics of cases 7B and 8 than with the constant settling velocity monodisperse suspension (case 1). Fig. 11 shows profiles of Reynolds stress and Reynolds flux for cases 1B, 7B and 8. Also, Fig. 12 shows the profiles of TKE production, dissipation and damping. All these figures clearly show that the statistics of case 7B and case 8 are in very good agreement. Similarly, we also present the *rms* velocity profiles of these three cases in Fig. 13. Although profiles for all the three cases are quite close to each other, the agreement between cases 7B and 8 is remarkable. Table 5 lists L2 norms of the difference in various turbulence statistics of case 7B from the monodisperse case 8. We will compare these norms with the L2 norms presented in Table 3 which correspond to the difference between cases 7B and 1B. Clearly, the L2 norms in Table 5 are at least an order of magnitude smaller. The most important differences are observed in statistics pertaining to sediment concentration. Here the L2 norms in Table 5 are at least 2 orders of magnitude smaller.

From the above discussion it is evident that the reason for such a good agreement between the monodisperse and polydisperse cases is the choice of sediment settling velocity specified inside the channel for the monodisperse case. Here the monodisperse settling velocity profile was extracted from the statistically stationary state of the polydisperse case. However, such information is not available a-priori and one would not know the precise form of $\tilde{V}_e$. Despite this apparent limitation, the simulation performed in this study demonstrates that turbulent statistics in turbidity current are primarily driven by the zeroth and first moments of a sediment suspension, which can be matched with a depth-dependent monodisperse suspension. In other words, a turbidity current with polydisperse suspension can be modeled by an effective monodisperse suspension which has a locally matching zeroth and first moment.

6. Conclusions

In this study we have presented a general mathematical formulation of turbidity currents driven by polydisperse sediment suspension. A simplification of the general framework was described where the population balance equation reduces to a set of scalar transport equations for discrete sediment sizes. This

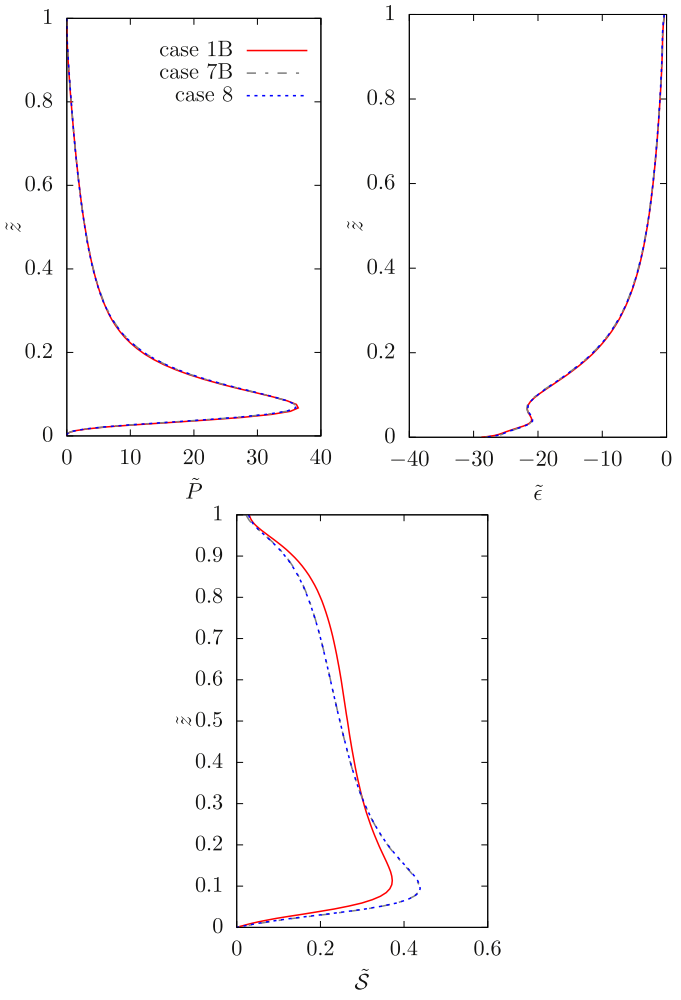

Fig. 12. Profiles of TKE production ($\tilde{P}$), TKE dissipation ($\tilde{\epsilon}$) and TKE damping ($\tilde{\mathcal{S}}$) for cases 1B, 7B and 8 (monodisperse suspension with variable settling velocity). We choose the settling velocity of the monodisperse suspension of case 8 inside the channel to be equal to the local effective settling velocity obtained for case 7B (see Fig. 9 and Eq. (49)).

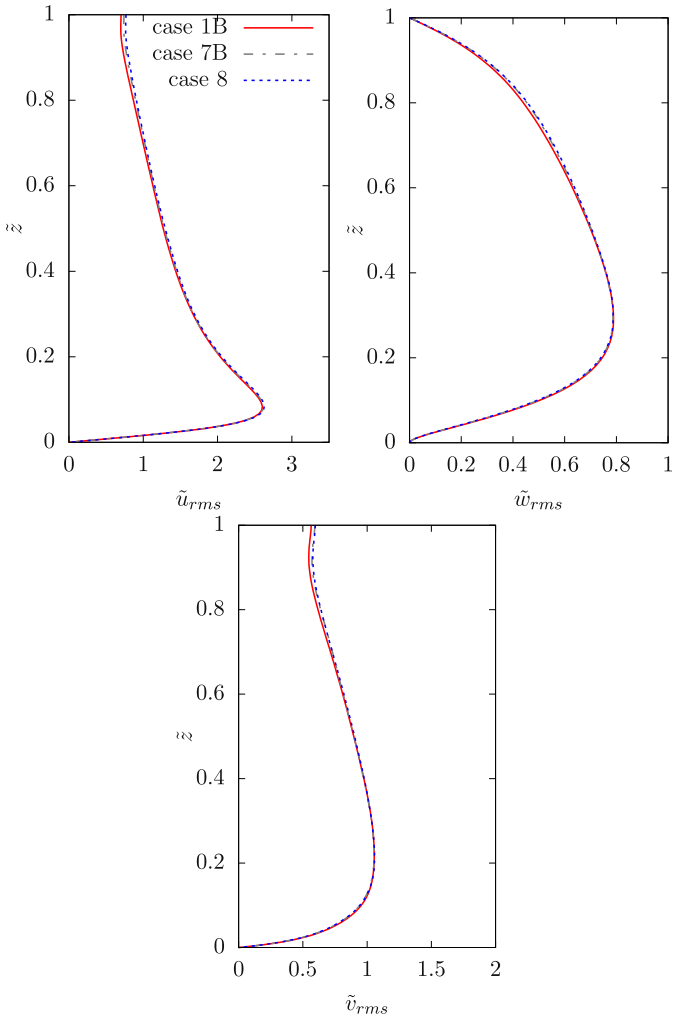

Fig. 13. Profiles of streamwise ($\tilde{u}_{rms}$), spanwise ($\tilde{v}_{rms}$) and wall normal ($\tilde{w}_{rms}$) *rms* velocity for cases 1B, 7B and 8 (monodisperse suspension with variable settling velocity). We choose the settling velocity of the monodisperse suspension of case 8 inside the channel to be equal to the local effective settling velocity obtained for case 7B (see Fig. 9 and Eq. (49)).

formulation was employed to perform simulations of turbidity currents in auto-suspension mode. In all the simulations $Re_\tau = 180$, $Sc = 1$ and $Ri_\tau = 11.42$ were held fixed and the composition of sediment suspension driving the flow was changed. Simulations were categorized into two sets A and B such that in each set the amount of sediment in suspension and the volume weighted average sediment settling velocity were maintained the same. In other words, in all the simulation cases within each set the zeroth and first moment of the sediment suspension based on fractional volume occupied by the different sediment sizes was held fixed. In each set, case 1 corresponds to the monodisperse suspension while the other cases contain more than one sediment size. We compare the turbulence statistics of the reference monodisperse case with the other polydisperse cases. It was observed that turbulence statistics, such as mean streamwise velocity, *rms* velocities, Reynolds stress, TKE production and TKE dissipation of case 1 (monodisperse suspension) adequately represent the corresponding statistics of the polydisperse cases in the set. However, statistics associated with sediment concentration, such as mean sediment concentration, Reynolds flux and TKE damping showed noticeable differences. It was also shown that these discrepancies arise because the monodisperse suspension with a constant sediment settling velocity cannot capture the local settling flux of polydisperse suspensions. To overcome this limitation we require a monodisperse suspension where the sediment settling velocity is allowed to vary in $\tilde{z}$ such that it represents the effective size of the local polydisperse suspension.

We performed a simulation of monodisperse suspension of sediment where the $\tilde{z}-$ dependent sediment settling velocity was obtained from the effective settling velocity of case 7B in the statistically stationary state. In other words, the settling velocity was a function of height from the bottom of the channel and its value was such that it captured the effective local sediment size in the flow. It is observed that with the depth-dependent settling velocity even the turbulence statistics associated with sediment concentration matched very well with the corresponding polydisperse case 7B. These results support the possibility that by matching the net sediment concentration and a depth-dependent first moment of a polydisperse sediment suspension it is possible to predict its behavior with an equivalent monodisperse current.

Acknowledgments

We wish to thank the National Science Foundation for Partnership for International Research and Education (PIRE) grant (NSF OISE-0968313) and NSF grant OCE-1131016.

Appendix A. Turbulent kinetic energy (TKE) equation

The ensemble averaged dimensionless turbulent kinetic energy equation corresponding to the stationary state of the flow is as shown below.

$$\tilde{P} - \tilde{\epsilon} + \tilde{T} + \frac{1}{Re_\tau}\frac{d^2 < \tilde{k} >}{dz^2} = -\sum_{m=1}^{N}\left\langle \tilde{u}'\tilde{c}_m'\right\rangle + Ri_\tau \sum_{m=1}^{N}\left\langle \tilde{w}'\tilde{c}_m'\right\rangle, \quad \text{(A.1)}$$

where

$$\tilde{k} = \frac{1}{2}\left(\tilde{u}'^2 + \tilde{v}'^2 + \tilde{w}'^2\right), \quad \tilde{P} = -\left\langle \tilde{u}'\tilde{w}'\right\rangle \frac{d\langle\tilde{u}\rangle}{d\tilde{z}}, \quad \text{(A.2)}$$

$$\tilde{\epsilon} = \frac{1}{Re_\tau}\left\langle \frac{\partial \tilde{u}_i'}{\partial \tilde{x}_j}\frac{\partial \tilde{u}_i'}{\partial \tilde{x}_j}\right\rangle \text{ and } \tilde{T} = \frac{d}{d\tilde{z}}\left(\left\langle \tilde{k}\tilde{w}'\right\rangle + \left\langle \tilde{p}'\tilde{w}'\right\rangle\right). \quad \text{(A.3)}$$

$\tilde{w}'\tilde{c}_m'$ is the Reynolds flux term which counters the sediment settling by mixing the sediment particles vertically in the channel. Reynolds flux is the mechanism by which sediment particles are held in suspension. From the concentration equation (22) we can write a balance equation for competing processes like Reynolds flux, settling flux and diffusive flux at the stationary state. This balance equation takes the form

$$-\tilde{V}_{mz}\frac{d\langle\tilde{c}_m\rangle}{d\tilde{z}} + \frac{d\langle\tilde{w}'\tilde{c}_m'\rangle}{d\tilde{z}} = \frac{1}{Re_\tau Sc}\frac{d^2\langle\tilde{c}_m\rangle}{d\tilde{z}^2}. \quad \text{(A.4)}$$

In the above $< >$ represents ensemble averaging, which is also equivalent to averaging in streamwise (x) and spanwise (y) direction owing to the periodic boundary conditions. Eq. (A.4) can be integrated in z direction to get a relation between settling flux, Reynolds flux and diffusive flux.

$$-\tilde{V}_{mz}\langle\tilde{c}_m\rangle + \left\langle\tilde{w}'\tilde{c}_m'\right\rangle = \frac{1}{Re_\tau Sc}\frac{d\langle\tilde{c}_m\rangle}{d\tilde{z}}. \quad \text{(A.5)}$$

Integration constant in the above expression drops out because at the walls Reynolds flux is absent and settling flux is exactly balanced by diffusive flux due to the enforced boundary condition. Now substitute (A.5) in (A.1) which gives

$$\tilde{P} - \tilde{\epsilon} + \tilde{T} + \frac{1}{Re_\tau}\frac{d^2 < \tilde{k} >}{d\tilde{z}^2} = -\sum_{m=1}^{N}\left\langle \tilde{u}'\tilde{c}_m'\right\rangle + Ri_\tau \sum_{m=1}^{N}\tilde{V}_{mz}\langle\tilde{c}_m\rangle + \frac{1}{Re_\tau Sc}\frac{d\langle\tilde{c}m\rangle}{d\tilde{z}}. \quad \text{(A.6)}$$

Integrating the above equation yields the TKE budget for the turbidity current.

$$\tilde{\mathcal{P}} - \tilde{\mathcal{E}} + \frac{1}{Re_\tau}\left(\left[\frac{d < \tilde{k} >}{d\tilde{z}}\right]_0^1 - \frac{1}{Sc}\sum_{m=1}^{N}[\tilde{c}_m]_0^1\right) = \tilde{\beta} + Ri_\tau \tilde{V}_e \cos\theta, \quad \text{(A.7)}$$

where

$$\tilde{\mathcal{P}} = \int_0^1 \tilde{P}d\tilde{z}, \tilde{\mathcal{E}} = \int_0^1 \tilde{\epsilon}d\tilde{z}, \tilde{V}_e = \int_0^1 \sum_{m=1}^{N}\tilde{V}_m\langle\tilde{c}_m\rangle d\tilde{z} = \sum_{m=1}^{N}\tilde{V}_{mz}\gamma_m, \quad \text{(A.8)}$$

$$\text{and} \quad \tilde{\beta} = -\sum_{m=1}^{N}\int_0^1 \left\langle\tilde{u}'\tilde{c}_m'\right\rangle d\tilde{z}. \quad \text{(A.9)}$$

Appendix B. Laminar solution

The governing equations (31)–(33) under the assumption of fully developed and steady flow reduces to

$$0 = \frac{1}{Re_\tau}\frac{d\tilde{u}}{d\tilde{z}} + \tilde{g}_x\sum_{m=1}^{N}\tilde{c}_m, \quad \text{(B.1)}$$

$$0 = -\frac{d\tilde{p}}{d\tilde{z}} + \tilde{g}_z\sum_{m=1}^{N}\tilde{c}_m, \quad \text{(B.2)}$$

$$\tilde{V}_{mz}\frac{d\tilde{c}_m}{d\tilde{z}} = \frac{1}{Re_\tau Sc}\frac{d^2\tilde{c}_m}{d\tilde{z}^2}. \quad \text{(B.3)}$$

Note that continuity and no penetration boundary condition leads to $\tilde{w} = 0$ and hence the z momentum equation reduces to pressure gradient balancing the hydrostatic potential. Eq. (B.3) can be integrated twice to get the laminar solution for sediment concentration in the channel.

$$\tilde{c}_m = \tilde{A}_m \exp\left(Re_\tau Sc\tilde{V}_m\tilde{z}\right) \quad \text{(B.4)}$$

The integration constant has to be determined from initial conditions, which is shown below

$$\int_0^1 \tilde{c}_m d\tilde{z} = \int_0^1 \tilde{A}_m \exp\left(Re_\tau Sc\tilde{V}_{mz}\tilde{z}\right)d\tilde{z} = \gamma_m. \quad \text{(B.5)}$$

Thus the integration constant can be written as

$$\tilde{A}_m = \frac{\gamma_m\left(Re_\tau Sc\tilde{V}_{mz}\right)}{\exp\left(Re_\tau Sc\tilde{V}_{mz}\right) - 1}. \quad \text{(B.6)}$$

Substituting (B.4) in the x momentum equation and integrating twice, we get

$$\tilde{u} = -Re_\tau\sum_{m=0}^{N}\frac{\tilde{A}_m}{Re_\tau Sc\tilde{V}_{mz}}\left[\frac{\exp\left(Re_\tau Sc\tilde{V}_{mz}\right)}{Re_\tau Sc\tilde{V}_{mz}} - \tilde{z}\exp\left(Re_\tau Sc\tilde{V}_{mz}\right) - \frac{1}{Re_\tau Sc\tilde{V}_{mz}}\right]. \quad \text{(B.7)}$$

Note that in the above solution, integration constants have been evaluated by applying no-slip and no stress boundary conditions on the bottom and top wall, respectively.

Appendix C. Higher order turbulence statistics and laminar solutions of set b

Various high order turbulence statistics like *rms* velocity, Reynolds stress, Reynolds flux, TKE production, TKE dissipation and TKE damping for set B are shown below. Laminar velocity and total sediment concentration profiles of all cases in set B are also provided (Figs. C.14–C.17)

Please cite this article as: M. Shringarpure et al., Equivalence of turbulence statistics between monodisperse and polydisperse turbidity currents, Advances in Water Resources (2017), http://dx.doi.org/10.1016/j.advwatres.2017.05.015

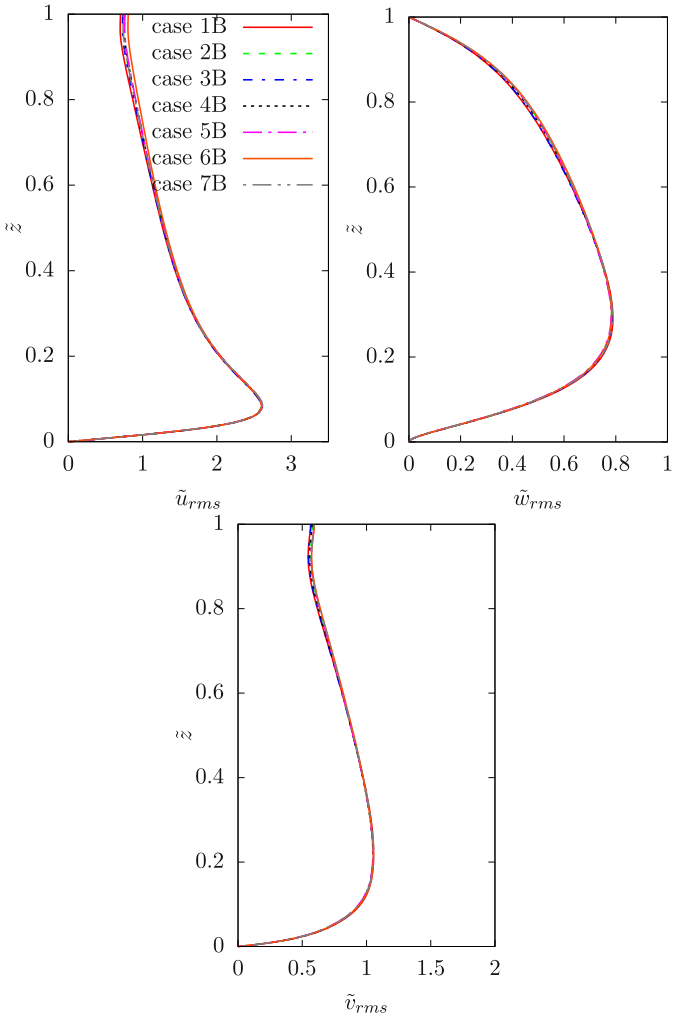

Fig. C.14. Profiles of streamwise ($\tilde{u}_{rms}$), spanwise ($\tilde{v}_{rms}$) and wall normal ($\tilde{w}_{rms}$) *rms* velocity for all cases in set B.

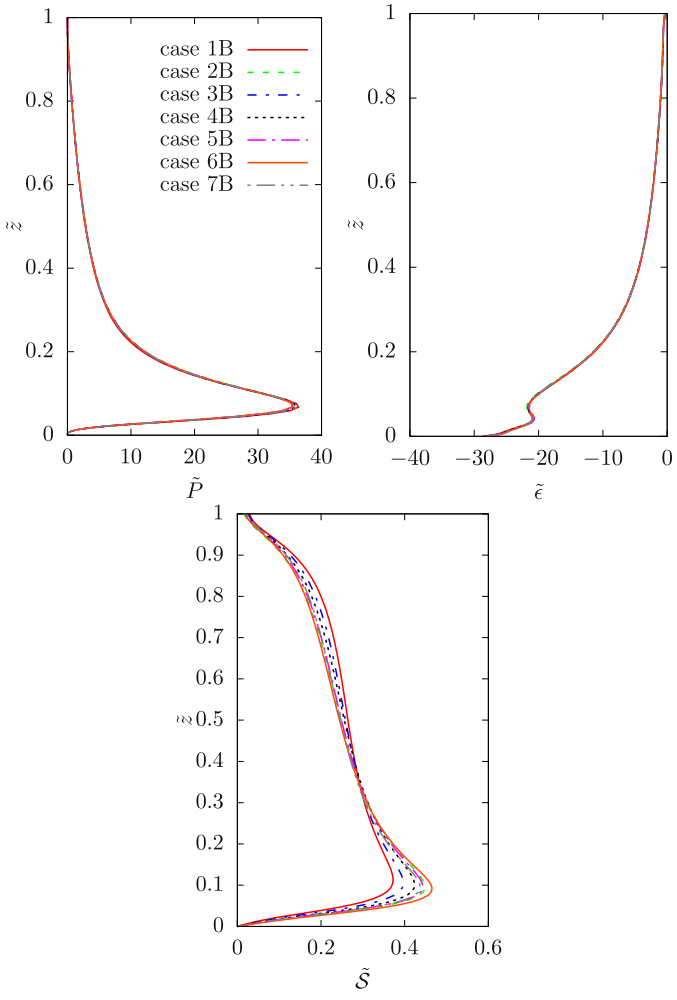

Fig. C.16. Profiles of TKE production ($\tilde{P}$), TKE dissipation ($\tilde{\epsilon}$) and TKE damping ($\tilde{\mathcal{S}}$) for all cases in set B.

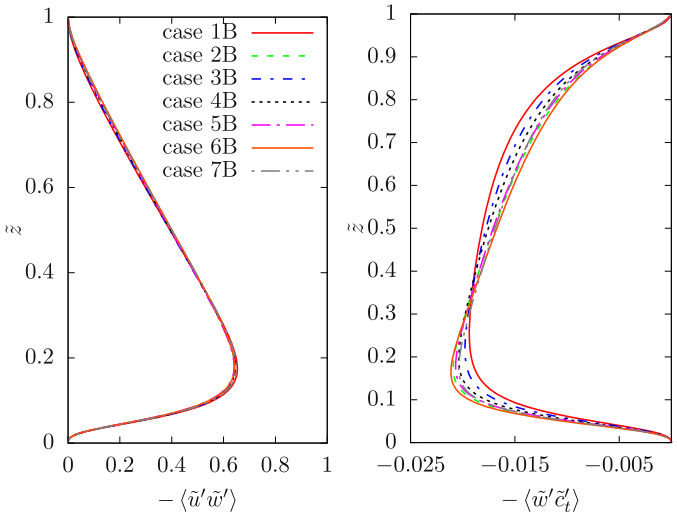

Fig. C.15. Profiles of Reynolds stress $\langle\tilde{u}'\tilde{w}'\rangle$ and Reynolds flux $\langle\tilde{w}'\tilde{c}_t'\rangle$ for all cases in set B.

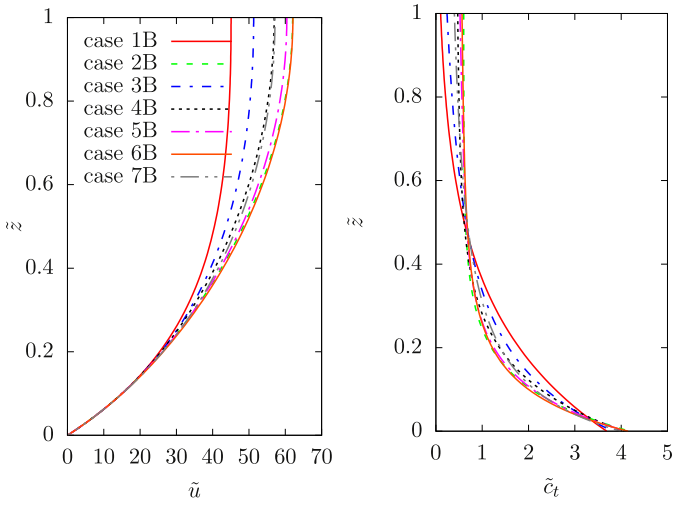

Fig. C.17. Profiles of streamwise velocity $\tilde{u}$ and total sediment concentration $\tilde{c}_t$ obtained from the laminar solution of the governing equations for all cases in set B.

References

Allen, J., 2001. Principles of Physical Sedimentology. The Blackburn Press.
Armenio, V., Sarkar, S., 2002. An investigation of stably stratified turbulent channel flow using large-eddy simulation. J. Fluid Mech. 459, 1–42.
Bagnold, R.A., 1962. Auto-suspension of transported sediment; turbidity currents. Proc. R. Soc. A 265, 315–319.
Balachandar, S., Eaton, J.K., 2010. Turbulent dispersed multiphase flow. Annu. Rev. Fluid Mech. 42, 111–133.
Bonnecaze, R.T., Hallworth, M.A., Huppert, H.E., Lister, J.R., 1995. Axisymmetric particle-driven gravity currents. J. Fluid Mech. 294, 99–121.
Bonnecaze, R.T., Huppert, H.E., Lister, J.R., 1996. Patterns of sedimentation from polydispersed turbidity currents. Proc. R. Soc. Lond. A 452 (1953), 2247–2261.
Cantero, M.I., Balachandar, S., Cantelli, A., Parker, G., 2014. A simplified approach to address turbulence modulation in turbidity currents as a response to slope breaks and loss of lateral confinement. Environ. Fluid Mech. 14 (2), 371–385. http://dx.doi.org/10.1007/s10652-013-9302-7.
Cantero, M.I., Balachandar, S., Cantelli, A., Pirmez, C., Parker, G., 2009. Turbidity current with a roof: direct numerical simulation of self-stratified turbulent channel flow driven by suspended sediment. J. Geophys. Res. Oceans 114.
Cantero, M.I., Balachandar, S., Garcia, M.H., 2007. High-resolution simulations of cylindrical density currents. J. Fluid Mech. 590, 437–469.
Cantero, M.I., Balachandar, S., García, M.H., 2008. An eulerian eulerian model for gravity currents driven by inertial particles. Int. J. Multiph. Flow 34, 484–501.
Cantero, M.I., Balachandar, S., García, M.H., Bock, D., 2008. Turbulent structures in planar gravity currents and their influence of the flow dynamics. J. Geophys. Res. Oceans 113.
Cantero, M.I., Balachandar, S., García, M.H., Ferry, J.P., 2005. Direct numerical simulations of planar and cylindrical density currents. J. Appl. Mech. 73 (6), 923–930.
Cantero, M.I., Balachandar, S., Parker, G., 2009. Direct numerical simulation of stratification effects in a sediment-laden turbulent channel flow. J. Turbul. 10, 1–28.
Cantero, M.I., Cantelli, A., Pirmez, C., Balachandar, S., Mohrig, D., Hickson, T.A., Yeh, T., Naruse, H., Parker, G., 2012. Emplacement of massive turbidites linked to extinction of turbulence in turbidity currents. Nat. Geosci. 5 (1), 42–45.
Cantero, M.I., Lee, J.R., Balachandar, S., Garcia, M.H., 2007. On the front velocity of gravity currents. J. Fluid Mech. 586, 1–39.
Cantero, M.I., Shringarpure, M., Balachandar, S., 2012. Towards a universal criteria for turbulence suppression in dilute turbidity currents with non-cohesive sediments. Geophys. Res. Lett. 39 (14). http://dx.doi.org/10.1029/2012GL052514.
Canuto, C., Hussaini, M., Quarteroni, A., Zang, T., 1988. Spectral Methods in Fluid Dynamics. Springer, New York.
Cortese, T.A., Balachandar, S., 1995. High performance spectral simulation of turbulent flows in massively parallel machines with distributed memory. Int. J. High Perform. Comput. Appl. 9, 187–204.
Das, H.S., Imran, J., Pirmez, C., Mohrig, D., 2004. Numerical modeling of flow and bed evolution in meandering submarine channels. J. Geophys. Res. Oceans 109 (C10), n/a–n/a. http://dx.doi.org/10.1029/2002JC001518. C10009.
Ferry, J., Balachandar, S., 2001. A fast eulerian method for disperse two-phase flow. Int. J. Multiph. Flow 27, 1199–1226.
Fukushima, Y., Parker, G., Pantin, H., 1985. Prediction of ignitive turbidity currents in scripps submarine canyon. Mar. Geol. 67 (1–2), 55–81. http://dx.doi.org/10.1016/0025-3227(85)90148-3.
García, M.H., 2008. Sedimentation Engineering: Processes, Measurements, Modeling and Practice, 3. ASCE, pp. 165–252.
Garcia, M., Parker, G., 1993. Experiments on the entrainment of sediment into suspension by a dense bottom current. J. Geophys. Res. 98, 4793–4807.
García, M.H., 1992. Turbidity Currents, 4. Academic Press Inc, pp. 399–408.
Hartel, C., Meiburg, E., Necker, F., 2000. Analysis and direct numerical simulation of the flow at a gravity-current head. Part 1. flow topology and front speed for slip and no-slip boundaries. J. Fluid Mech. 418, 189–212. http://dx.doi.org/10.1017/S0022112000001221.
Imran, J., Kassem, A., Khan, S.M., 2004. Three-dimensional modeling of density current. i. flow in straight confined and unconfined channels. J. Hydr. Res. 42 (6), 578–590. http://dx.doi.org/10.1080/00221686.2004.9628312.
Kneller, B., Bennett, S., McCaffrey, W., 1997. Velocity and turbulence structure of density currents and internal solitary waves: potential sediment transport and the formation of wave ripples in deep water. Sediment. Geol. 112 (3), 235–250. http://dx.doi.org/10.1016/S0037-0738(97)00031-6.
Kneller, B., Buckee, C., 2000. The structure and fluid mechanics of turbidity currents; a review of some recent studies and their geological implications. Sedimentology 47, 62–94.
Krause, D., White, W., Piper, D., Heezen, B., 1970. Turbidity currents and cable breaks in the western new britain trench. Geol. Soc. Am. Bull. 81, 2153–2160.
Marchisio, D.L., Fox, R.O., 2005. Solution of population balance equations using the direct quadrature method of moments. J. Aerosol. Sci. 36 (1), 43–73. http://dx.doi.org/10.1016/j.jaerosci.2004.07.009.
Middleton, G.V., 1976. Hydraulic interpretation of sand size distributions. J. Geol. 84 (4), 405–426. http://dx.doi.org/10.1086/628208.
Mucha, P.J., Brenner, M.P., 2003. Diffusivities and front propagation in sedimentation. Phys. Fluids 15 (5), 1305–1313. http://dx.doi.org/10.1063/1.1564824.
Nasr-Azadani, M., Hall, B., Meiburg, E., 2013. Polydisperse turbidity currents propagating over complex topography: comparison of experimental and depth-resolved simulation results. Comput. Geosci. 53, 141–153. http://dx.doi.org/10.1016/j.cageo.2011.08.030. Modeling for Environmental Change.
Nasr-Azadani, M.M., Meiburg, E., 2014. Turbidity currents interacting with three-dimensional seafloor topography. J. Fluid Mech. 745, 409–443. http://dx.doi.org/10.1017/jfm.2014.47.
Necker, F., Hartel, C., Kleiser, L., Meiburg, E., 2005. Mixing and dissipation in particle-driven gravity currents. J. Fluid Mech. 545, 339–372.
Pantin, H.M., 1979. Interaction between velocity and effective density in turbidity flow - phase-plane analysis, with criteria for autosuspension. Mar. Geol. 31 (1–2), 59–99.
Pantin, H.M., Franklin, M.C., 2009. Predicting autosuspension in steady turbidity flow: ignition points and their relation to richardson numbers. J. Sediment. Res. 79 (11–12), 862–871. http://dx.doi.org/10.2110/jsr.2009.095.
Parker, G., Fukushima, Y., Pantin, H., 1986. Self-accelerating turbidity currents. J Fluid Mech 171, 145–181.
Parsons, J.D., Friedrichs, C.T., Traykovski, P.A., Mohrig, D., Imran, J., Syvitski, J.P.M., Parker, G., Puig, P., Buttles, J.L., García, M.H., 2009. The mechanics of marine sediment gravity flows. Blackwell Publishing Ltd., pp. 275–337.
Patterson, M.D., Simpson, J.E., Dalziel, S.B., van Heijst, G.J.F., 2006. Vortical motion in the head of an axisymmetric gravity current. Phys. Fluids 18 (4), 046601. http://dx.doi.org/10.1063/1.2174717.
Pinet, P.R., 2006. Invitation to Oceanography, 4 Jones and Bartlett.
Prior, D.B., Bornhold, B.D., Wiseman, W.J., Lowe, D.R., 1987. Turbidity current activity in a british columbia fjord. Science 237 (4820), pp.1330–1333.
Ramkrishna, D., 2000. Population Balances: Theory and Applications to Particulate Systems in Engineering. Academic Press.
Ramkrishna, D., Singh, M.R., 2014. Population balance modeling: current status and future prospects. Annu. Rev. Chem. Biomol. Eng. 5 (1), 123–146. http://dx.doi.org/10.1146/annurev-chembioeng-060713-040241. PMID: 24606333.
Salinas, J.S., Shringarpure, M., Cantero, M.I., Balachandar, S., 2017. Mixing at a sediment concentration interface in turbulent open channel flow. Environ. Fluid Mech, pp. 1–28. http://dx.doi.org/10.1007/s10652-017-9521-4. Special issue on Environmental buoyancy-driven flows.
Segre, P.N., Liu, F., Umbanhowar, P., Weitz, D.A., 2001. An effective gravitational temperature for sedimentation. Nature 409, 594–597.
Sequeiros, O., Naruse, H., Endo, N., García, M., Parker, G., 2009. Experimental study on self-accelerating turbidity currents. J. Geophys. Res. 114.
Sequeiros, O., Spinewine, B., Beaubouef, R., Sun, T., García, M., Parker, G., 2010. Characteristics of velocity and excess density profiles of saline underflows and turbidity currents flowing over a mobile bed. J. Hydraul. Eng. 136, 412–433.
Shringarpure, M., Cantero, M.I., Balachandar, S., 2012. Dynamics of complete turbulence suppression in turbidity currents driven by monodisperse suspensions of sediment. J. Fluid Mech. 712, 384–417. http://dx.doi.org/10.1017/jfm.2012.427.
Shringarpure, M., Cantero, M.I., Balachandar, S., 2014. Mechanisms of complete turbulence suppression in turbidity currents driven by mono-disperse and bi-disperse suspensions of sediment. J. Comput. Multiph. Flows 6 (3), 221–246.
Shringarpure, M., Cantero, M.I., Balachandar, S., 2015. Analysis of turbulence suppression in sediment-laden saline currents. Procedia Eng. 126, 16–23. http://dx.doi.org/10.1016/j.proeng.2015.11.170. Frontiers in Fluid Mechanics Research.
Simpson, J.E., 1997. Gravity Currents: In the Environment and the Laboratory, 2nd Cambridge University Press.
Talling, P.J., Wynn, R.B., Masson, D.G., Frenz, M., Cronin, B.T., Schiebel, R., Akhmetzhanov, A.M., Dallmeier-Tiessen, S., Benetti, S., Weaver, P.P.E., Georgiopoulou, A., Zuhlsdorff, C., Amy, L.A., 2007. Onset of submarine debris flow deposition far from original giant landslide. Nature 450, 541–544.
Taylor, J.R., Sarkar, S., Armenio, V., 2005. Large eddy simulation of stably stratified open channel flow. Phys. Fluids 17 (11), 116602. http://dx.doi.org/10.1063/1.2130747.
Ungarish, M., 2009. An Introduction to Gravity Currents and Intrusions. Chapman and Hall/CRC Press.
Xu, J.P., Noble, M.A., Rosenfeld, L.K., 2004. In-situ measurements of velocity structure within turbidity currents. Geophys. Res. Lett. 31 (9). http://dx.doi.org/10.1029/2004GL019718.
Zonta, F., 2013. Nusselt number and friction factor in thermally stratified turbulent channel flow under non-Oberbeck–Boussinesq conditions. Int. J. Heat Fluid Flow 44, 489–494. http://dx.doi.org/10.1016/j.ijheatfluidflow.2013.08.007.
Zonta, F., Onorato, M., Soldati, A., 2012. Turbulence and internal waves in stably-stratified channel flow with temperature-dependent fluid properties. J. Fluid Mech. 697, 175–203. http://dx.doi.org/10.1017/jfm.2012.51.
Zonta, F., Soldati, A., 2013. Effect of temperature dependent fluid properties on heat transfer in turbulent mixed convection. J. Heat Transf. 136 (2), 022501–022501–12.

Please cite this article as: M. Shringarpure et al., Equivalence of turbulence statistics between monodisperse and polydisperse turbidity currents, Advances in Water Resources (2017), http://dx.doi.org/10.1016/j.advwatres.2017.05.015